

Contents

1. Ice velocity measured by differential GPS	2
1.1. Introduction	2
1.2. Theoretical background	3
1.3. Methods and setup	7
1.3.1. Methods	7
1.3.2. Setup	8
1.4. Processing	9
1.4.1. Trimble	9
1.4.2. Open source	10
1.4.3. Stake correction	14
1.4.4. Evaluation	16
1.4.5. Propagation of uncertainty	16
1.4.6. Final positions	18
1.5. Results	20
1.5.1. Horizontal velocity (ice flow)	20
1.5.2. Vertical velocity (mass balance)	22
1.5.3. Theoretical surface velocity	28
1.6. Discussion	29
1.6.1. Horizontal velocity	29
1.6.2. Vertical velocity	32
1.7. Conclusion	32
Bibliography	34
Appendices	35
A. Appendix Ice velocity	36

1. Ice velocity measured by differential GPS

Abstract

The aim of this report is to measure the ice velocity of the glaciers Tellbreen and Blekumbreen (Adventdalen, Svalbard) with the differential Global Positioning System (dGPS) method. This method with a higher accuracy than the Global Positioning System (GPS) is necessary to deal with very small velocities. A new open-source post-processing method is applied and suggestions of long-term and convincing replacement of the former method are provided to slowly transition away from the restricted Trimble Business Center post-processing work-flow. The average uncertainties of our measured positions are 40 cm for Northing, 19 cm for Easting and 89 cm for the elevation. As such they are larger than the calculated yearly displacements, making it very difficult to determine the ice velocity for all stakes on either of the two glaciers. This conclusion induces an irrelevancy to perform further calculation on the ice fluxes and their directions. The mass balance of the glacier is calculated through the change of elevation in time at each stake. The mass balance gradient is 5.1 ± 1.0 mm/m on Tellbreen and 6.8 ± 1.4 mm/m on Blekumbreen. The altitudes of the theoretical equilibrium lines at 757 ± 56 m for Tellbreen and 751 ± 45 m for Blekumbreen are higher than the highest point of any of the two glaciers. Both glaciers are situated in their own ablation zone. We verify our velocity calculations with the theoretical model of the *shallow ice* approximation. The theoretical velocity values have orders of magnitude of centimeters per year for reasonable assumptions of slope angles, ice viscosities and ice thicknesses. Their results confirm our measurement results with a slow movement of both glaciers.

1.1. Introduction

Many topics in glaciology call for an understanding of the velocity field in a glacier. In fact, the way in which the flow redistributes mass is directly connected to a glacier's shape. But flow also induces energy redistribution and as such, the temperature distribution, which itself has implications for the nature of the coupling with the glacier bed. Spatial variations in speed, also known as strain rates ϵ , are being studied by structural geologists who use glaciers as analogs for rock deformation. From a geomorphic point of view as well, the entrainment of debris and the different moraines they construct depend upon the flow field too. Understanding those velocity fields therefore is fundamental to the analysis of a number of problems in glacier mechanics. In this experiments aiming at ice velocities and fluxes, we used the differential Global Positioning System (dGPS) to collect accurate data at the mass balance stakes' positions. Relying on these measurements to extract experimental values for the surface velocity of the glacier, we compared previous positions from the last years to the new ones. We also particularly dedicated our attention

towards the data treatment algorithms, as a clear understanding of the processing appears to be fundamental in an experiment with very sensitive devices and potential for large latent errors. In that scope, we introduced a new method based on an open-source post-processing that allows a transparent step-by-step understanding of the work-flow. For consistency however, we kept conducting the Trimble Business Center post-processing next to our new design, be it only to ensure continuity with the previous years' results. We focused on the measurement method because the results from the previous years seemed to be rather unclear or unreliable, and could hence not provide a real movement of the glacier. We therefore thought important to emphasize on the analysis of the measurement methods and their uncertainties, and herewith suggest a more rigorous protocol aiming at a more durable and reliable data collection on the field in the upcoming editions of this experiment.

The chapter on Theory walks us through the calculation of the horizontal velocity in a glacier. After having motivated the computation of the surface velocity through the *shallow ice* approximation, we relate it to a depth-averaged velocity. Using this result, we present a value for the ice flux per unit width. Finally, we cross-check our results with those of the mass-balance group and draw a conclusion rejecting the *steady state* assumption. In the Processing chapter, the stake's effective positions are determined by the post-processing relying on base-station data and the stake's corrections. The latter is motivated by measurements of inclination and height that revealed the importance and necessity of considering the propagation of uncertainties. With the position data including Northing, Easting and elevation, the velocity of every stake can be calculated both through the theory and by taking the difference between the stakes' positions of the last years. It is here that support provided by the data of the ice-radar group is determining ; we use the ice thickness that they extrapolated from their glacier scanning to provide a comparative theoretical value to the experimental surface velocity. Next to the horizontal velocity, it was possible to calculate the vertical velocity to determine a mass balance for our measurement sites. Finally, the discussion and conclusion close the report.

1.2. Theoretical background

Ice velocities using the stake positions of the previous year

If we define each measured position of the mass balance stakes by $P_i(x, y, z)$ where P accounts for the codename of the stake and i labels the year of the considered stake, the horizontal distance d between a stake $P_a(x_a, y_a, z_a)$ and $P_b(x_b, y_b, z_b)$ is given by :

$$d = \sqrt{(x_a - x_b)^2 + (y_a - y_b)^2} \quad (1.1)$$

The horizontal surface velocity u_s is calculated through :

$$\boxed{u_s = \frac{d}{t_{a \rightarrow b}}} \quad (1.2)$$

where $t_{a \rightarrow b}$ is the elapsed time between the measurements a and b .

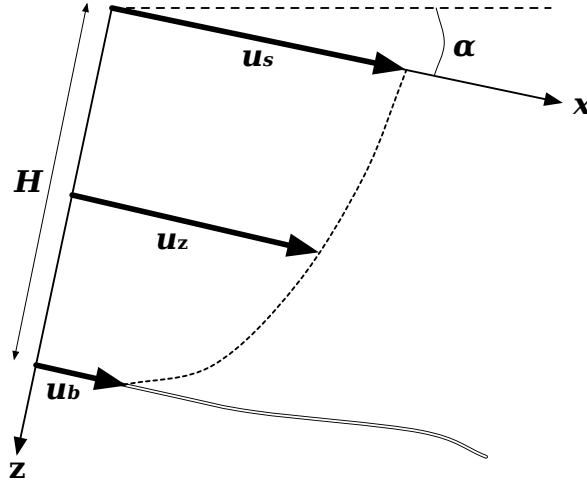


Figure 1.1.: Schematic diagram of our velocity profile

Relating the surface velocity to depth-averaged ice velocity

Now that we have the horizontal surface velocity, we wonder how it evolves with depth. J. F. Nye (1952) has proven that the overlying ice of a glacier must move at least as fast as that below. In quantitative terms, this translates to a reasoning that starts with the flow law for the strain rate $\dot{\epsilon}$:

$$\dot{\epsilon} = \left(\frac{\sigma}{B} \right)^n \quad (1.3)$$

with σ a dominant shear stress, B an ice viscosity parameter that is temperature dependent and increases with the stiffness of the ice, and n the constant creep exponent. The latter has often experimentally proven to be $n \approx 3$, but for the sake of the derivation, we'll keep the value variable. This law is also named after Glen's J. W. Glen (1955), who conducted the first uniaxial compression experiments on ice.

We will follow up with the assumptions of the layer we consider being parallel-sided, that there's no flow in y direction and that everything is uniform in x, y , as depicted in the FIGURE 1.1. The stress rate tensor therefore comes down to :

$$\dot{\epsilon} = \begin{pmatrix} 0 & 0 & \dot{\epsilon}_{xz} \\ 0 & 0 & 0 \\ \dot{\epsilon}_{zx} & 0 & 0 \end{pmatrix} \quad (1.4)$$

From the constitutive relations, linking the stress σ to the strain ϵ component per component, it follows that $\sigma_{xz} = \sigma_{zx}$ and hence :

$$\dot{\epsilon}_{zx} = \left(\frac{\sigma_{zx}}{B} \right)^n \quad (1.5)$$

By the property $\dot{\epsilon}_{xy} = \frac{1}{2} \left(\frac{\partial u}{\partial y} + \frac{\partial v}{\partial x} \right)$, assuming the shear to take place in the plane normal to z so that $\partial w / \partial x = 0$ and the stress configuration to be of simple shear, the last equation becomes :

$$\frac{du}{dz} = 2 \left(\frac{\sigma_{zx}}{B} \right)^n \quad (1.6)$$

We can express σ_{zx} as a function of z by using the coordinate system of FIGURE 1.1 and noticing that $\sigma_{zx} = -\rho g h \sin \alpha$. After that, integration from the surface to the depth z becomes possible :

$$\int_{u_s}^{u(z)} du = -2 \left(\frac{\rho g \sin \alpha}{B} \right)^n \cdot \int_0^z z^n dz \quad (1.7)$$

The depth-averaged ice velocity appears after carrying out the integration and rearranging the terms as conducted in Hooke (2005) :

$$u(z) = u_s - \frac{2}{n+1} \left(\frac{\rho g \sin \alpha}{B} \right)^n \cdot z^{n+1} \quad (1.8)$$

This value becomes computable as soon as we know u_s , B and α . If we also know the total thickness H , the last equation becomes solvable at the bed and we get the bedrock velocity u_b :

$$u_b = u_s - \frac{2}{n+1} \left(\frac{\rho g \sin \alpha}{B} \right)^n \cdot H^{n+1} \quad (1.9)$$

Our derivation here only is rigorously correct for a slab-shaped glacier of an infinite extent on a uniform slope. If for instance the glacier is bounded laterally, we will have to consider drag on the sides when calculating σ_{zx} :


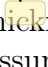
$$\sigma_{zx} = -S_f \rho g z \sin \alpha \quad (1.10)$$

where we have introduced the shape factor S_f ; we possess tables of values for different shapes, but it's good to remember that S_f is 1 for an infinitely wide glacier, and $1/2$ for a semicircular glacier.

With that addition, our depth-averaged ice velocity finally reads :

$$u(z) = u_s - \frac{2}{n+1} \left(\frac{S_f \rho g \sin \alpha}{B} \right)^n \cdot z^{n+1} \quad (1.11)$$

The *shallow ice* approximation and theory-motivated velocity

This approximation concerns large ice sheets where conditions generally  little over horizontal distances of 5-10 times the local ice thickness  Greve (2009). Ice flow then becomes determined by local conditions such as ice thickness, surface inclination and temperature. In addition to this, we add some further assumptions :

- our bedrock shall be *flat* throughout our measurements
- the bedrock shall be frozen, and hence : $u_b = 0$

With this basis, the previously derived expression for the base velocity u_b becomes :

$$u_b = 0 = u_{\textcircled{S}} - \frac{2}{n+1} \left(\frac{\rho g \sin \alpha}{B} \right)^n \cdot H^{n+1} \xrightarrow{n=3} \boxed{u_{\textcircled{S}} = \frac{1}{2} \left(\frac{\rho g \sin \alpha}{B} \right)^3 \cdot H^4} \quad (1.12)$$

where $u_{\textcircled{S}}$ uses the circled subscript for the theory-motivated value of the ice velocity. We will keep using u_s for the sake of generalization, but our theoretical computations in the next chapter will invoke this newly presented $u_{\textcircled{S}}$.

Calculating the ice flux through an arbitrary cross section profile

From definition, the ice flux per unit width q is obtained by integrating the velocity profile over depth :

$$q = \int_0^H u(z) dz = u_s H - \frac{2}{(n+1)(n+2)} \left(\frac{S_f \rho g \sin \alpha}{B} \right)^n \cdot H^{n+2} \quad (1.13)$$

Introducing at this stage the mean velocity over depth $\bar{u} \equiv q/H$ reveals to be of greater advantage :

$$\bar{u} = u_s - \frac{2}{(n+1)(n+2)} \left(\frac{S_f \rho g \sin \alpha}{B} \right)^n \cdot H^{n+1} \quad (1.14)$$

From here, after some calculus appears the very ergonomic expression :

$$\bar{u} = \frac{4}{5} u_s + \frac{1}{5} u_b = \frac{4}{5} u_{\textcircled{S}} \quad (1.15)$$

This last expression allows us to jump back to a formula for the ice flux, reversing the definition of the mean velocity :

$$\boxed{q = \bar{u} H = \frac{4}{5} u_{\textcircled{S}} H} \quad (1.16)$$

Mass balance and the *steady state* assumption

The massive ice flux per unit width can be defined through :

$$q_m = \bar{\rho} q \quad (1.17)$$

where $\bar{\rho}$ is the vertically averaged density.

If we define an arbitrary planar cross-section A of width W around the positions where we measured u_s , and introduce the mass M of the volume area comprised by $A \cdot H$, then the rate at which it changes would usually be defined K. M. Cuffey (2010) by :

$$\frac{dM}{dt} \equiv \bar{\rho} \int_A \dot{b}_i dA - \int_W q_m dW \quad (1.18)$$

where \dot{b}_i is the ice-equivalent specific mass balance rate in $[\text{m}/\text{yr}]$. If we know the direction of the flow, it then becomes easier to pick a arch of width W across the glacier into which A would flow. We shall discover later that this is particularly difficult on both Tellbreen and Blekumbreen, partly because of the small order or magnitude of the

measured velocities, which is in accordance with our further theoretical computations, but also because of the quite incoherent positioning over the years of the moving stakes, which makes it impossible to pick a favorite direction for the flux.

Yet if we decide to set the velocity to be zero as a prolongation of our experimental observation and predictions from the theory, then we'd have :

$$\boxed{\frac{dM}{dt} \stackrel{u_s=0}{=} \bar{\rho} \int_A \dot{b}_i dA} \quad (1.19)$$

In the first order of approximation, should the right-hand side be anything else than zero, this equality would allow us to deny the *steady state* assumption as any non-zero value to be multiplied by $\bar{\rho}$ and integrated over an area A would mean a mass changing rate in the glacier.

1.3. Methods and setup

1.3.1. Methods

The aim of this report is to measure the ice velocity of the two glaciers at different points. The points are consistently given by the mass balance stakes as a reference to the last years. The velocity will be calculated by the position difference of the stakes as a function of time. Regarding to the results of the previous years, it is given that the ice velocity for the glaciers Tellbreen and Blekumbreen is less than one meter. The position measurements during the fieldwork are made with GPS. The general used GPS system has only an accuracy in the order of meters. By correcting the measurement data with the data from a base station, it is possible to have a more accurate positioning to the order of millimeters (Kaplan and Hegarty, 2005). This method is named dGPS.

The GPS signal is broadcast with two certain frequencies L1 and L2 which belongs to two different services. The transmission signals with L1 and L2 are the carrier component, which is one component of the Global Navigation Satellite System (GNSS) structure the GPS receivers are using. In the GNSS there are 24 operational plus some redundant satellites available. There are five different GNSS constellations (GPS, GLONASS, QZSS, COMPASS and Galileo), which can be used for measurements (Trimble Survey division, 2012). To reach the satellites the signal has to go through the different atmospheric layers (Churcher, 2011), because the orbit of the satellites is approximately 20000 km over the earth surface (Trimble Survey division, 2012).

The Real-time Kinematic (RTK) positioning has the concept to remove errors based on the comparison to the base station. When the position of the satellite is known, the position of the receiver is calculated by trilateration based on the measured distance between receiver and each satellite. The position of the satellite is broadcast as an ephemerides, which is a specific positioning. The errors from the GPS measurements that are corrected by the dGPS method are correlated in time and space. So the identified errors can be assumed to be the same at the receiver as at the base station. The disturbances can be distinguished, because the position of the base station is very well known. The realisation of the GPS error correlation between two receivers with a specific distance can be defined as a baseline. Also a time correlation is meaningful, because there is always a time delay in the data transfer possible. Possible disturbances can be caused by satellite clock

errors, ephemeris errors, tropospheric errors (variation of the speed of electromagnetic radiation), ionospheric errors (dependent on signal frequency, elevation angle and the total electron content). There are also the receiver noise and multipath as a uncorrelated error source between the two receivers (Kaplan and Hegarty, 2005). For reducing the errors by different sources the receiver need a additional source with precise positions, clock offsets and good correction of atmospheric disturbances. Differential positioning is used to reduce the errors by orbit and atmosphere, which are similar for both receiver as long as the distance in between is not too long (Trimble Survey division, 2012). For further information it is to recommend to read in the referenced book of (Kaplan and Hegarty, 2005).

The GPS measurements have been done with the Trimble differential Global Navigation Satellite System (GNSS). The measured parameters were the northing and easting as well as the elevation. The accuracy of the dGPS is decreasing with a increasing distance to the base station and differs between the horizontal and the vertical component. For the Fast Static method the horizontal accuracy is $\pm 3 \text{ mm} + 0.1 \text{ ppm}$ and vertical $\pm 3.5 + 0.4 \text{ ppm}$ (Gölles, 2012). But this uncertainty is at least one order of magnitude smaller than the other uncertainties and can be neglected. The setting during our measurements included the receiver Trimble R4, the controller Trimble TCS2 and a carbon pole to mount the receiver properly. During the operation of the measurements we followed exact the description in section 2 and 3 in Gölles (2012). The recommended Fast Static survey method is used. The used coordinate system is the Universal Transversal Mercator (UTM) for the zone 33X with WGS 1984 date (Gölles, 2012).

So the disturbances by the atmosphere during the measuring time can be corrected while the measured coordinates are compare on every timestep defined by the GPS time. The further steps of the post processing is explained in the next section 1.4. We also did two measurements at the same stake on two different days to see how the results are effected. The duration for our measurements with the GPS receiver was at least 15 minutes. We had to made a trade off between the quality of the result and the total number of measurements to measure all stakes at least one time. With a longer measurement time the statistical fluctuations are better averaged out.

The analysis in this report is made with python.

1.3.2. Setup

The setup for our measurements is specified by a guideline to insure that the measurements are consistent during the whole fieldwork. In the following text the mass balance stake is only named as stake and the pole with the Trimble receiver will be shortend to the name rover. The receiver on the carbon pole has to be positioned, in the best scenario, on the top of the mass balance stake. To determine the uncertainty from a tilted stake, it is necessary to measure the inclination of the stake as well as the direction of inclination with the compass. The snow depth is measured with the probe which has a centimeter scale on it. With snow depth and the antenna height the actual height over the ice surface is known. When the stake is already melted out too high, it is necessary to put the pole with the rover next to the stake. In this case the poles has to be positioned northwards of the stake so that the correction is only in the northing component, which makes the calculation easier. Also the distance from the receiver to stake is measured. These two

different setups are shown in photographs in the figure 1.2.



Figure 1.2.: Setup while the GPS measurement next to the stake (left) and on top of the stake (right).

1.4. Processing

The post processing is based on the correction of the measurement data. In the first part of the processing the base station data are used to get a higher accuracy of the GPS data. The nearest base station is Statens Kartverks SatRef located on Platåberget with a distance between 14 km and 20 km depending on the mass balance stake. The second part of the processing contains the stake correction based on the measurements.

In the previous reports the post processing was done with the commercial software Trimble Business Center (TBC). In this report we use a new method for the post processing. This method is an open source (OS) alternative which is available for different system softwares and is usable without a license. The TBC is only available on a windows system and needs a licence. This leads to a limitation in the application. We operate both methods to quantify if the TBC method can be replaced by the OS method without an offset in the positioning.

1.4.1. Trimble

While the TBC post processing all mentioned steps from section 5 Gölles (2012) are done. For each day the data file from the measurements and the corresponding base station data file is imported. The data are available for the days of year(doy) 070, 072, 074 and 075. All data files from the base station are in the .o18-format and downloaded from the server

of Statkart server. The data from the rover have the .t02 format. After the TBC post processing the results from the are stored in a .csv-file.

The GNSS processing in the TBC use the combination of base station and rover data. The goal is to “fix” the number of whole wavelengths between the rover and satellites. This process is done in two steps by generating a ‘float’ solution and resolve an integer value, the integer ambiguity. If a solution is successfully it is defined as ‘fixed’. The transition from ‘float’ to ‘fixed’ is the initialization period. A slower convergence of the solution as normal is possible for longer baselines or when the signal is blocked by objects in the surrounding. After some amount of time the float solution can switch instantaneously to a fixed solution. There is also a disadvantage of the float and fixed approach for integer ambiguity resolution. At some point in time the convergence to fixed solution is slow and impossible to change. By mistake a wrong fixed value can be set, which can lead to an abnormal high position error due to an incorrect set of integer ambiguities. During the processing the TBC use automatically the best way to measure and correct the position data. The change of the method is for example dependent on the length of the baseline. Baselines are determined by the distance between rover and base station. For longer baselines the uncertainties have to be reduced with an additional approach, like a model. For different settings and situations the TBC used different approaches for the tropospheric and ionospheric uncertainties and choose automatically the best combination (Trimble Survey division, 2012). Therefore it is difficult to distinguish the settings used for the TBC post processing to apply on the OS processing.

1.4.2. Open source

The OS post processing requires different processing steps. First of all the raw data file has to be transformed from the original Trimble format .t02 to a data file in .tdg-format, because .t02-files are not readable for the OS post processing programs. This transformation was done with the program runpkr00 which is available on the website of unavco <http://kb.unavco.org/kb/article/trimble-runpkr00-v5-40-latest-version-mac-osx-10-7-windows-xp-7-linux-solaris-744.html>. The used command is

```
runpkr00 -g -d filename.t02
```

Due to problems with the package it was necessary to do a manual transformation of the package. To provide the correct file format for the last post processing step we use the toolkit teqc. This toolkit is also available on the website of unavco <https://www.unavco.org/software/data-processing/teqc/teqc.html>. Then the file can be converted to an observation (.obs) and navigation (.nav) file by the command

```
./teqc +nav filename.nav +obs filename.obs filename.tgd.
```

After this step it is necessary to download the base station data from the server of Statkart <http://ftp.statkart.no/> in the .18n-format for the doy 070, 072, 074 and 075.

The final step in the OS post processing of the GPS data is done with the open source program package RTKLIB. This package is available for the download in the website <http://www.rtklib.com/rtklib.htm>. In this package we use the executable rtkpost.exe of the downloaded full package with source Programs in the up-to-date version 2.4.2. In this software the two navigation file from the receiver and the base station as well as the

observation file from the receiver has to be read in. The .n18-format from the base station is a comparable navigation file to the navigation file from the receiver date. To execute RTKPOST it is required to adjust the appropriate settings. For all stakes the settings in the post processing were the same. The settings are displayed in the header of the output file. The header with the settings for the OS post processing is available in the appendix A. The settings are as similar as possible to the TBC settings. But due to the automatic adjustment to the best correction in the TBC it is difficult to find the same set of settings. In the OS post processing different correction methods for the tropospheric and ionospheric correction are available to choose. Due to missing informations from TBC the probably best method was chosen with 'broadcast' correction for the ionosphere and the 'saastamoinen' correction for optimize the accuracy due to tropospheric errors. The other settings can be taken from the header information to reproduce the OS post processing. The final output after the post processing is a position file (.pos). The results of the OS post processing are given as a time series of latitude, longitude and elevation. where

Because the UTM coordinate system is consistently used in our report the horizontal components are transformed to the UTM coordinate system by a python function. To get one position, including northing, easting and elevation value in m, the weighted mean of the standard deviation of this time series is calculated over all time steps.

17

Unknown

18

4/30/18

Chris Borstad



19-20

2 notes:

Without the correction of the base station data the values for northing, easting and elevation fluctuate with a high frequency due to a lot of disturbances (compare subsection 1.3.1). Exemplary, this time series is shown in Figure 1.3 for the first measurement of the stake T1-2017.



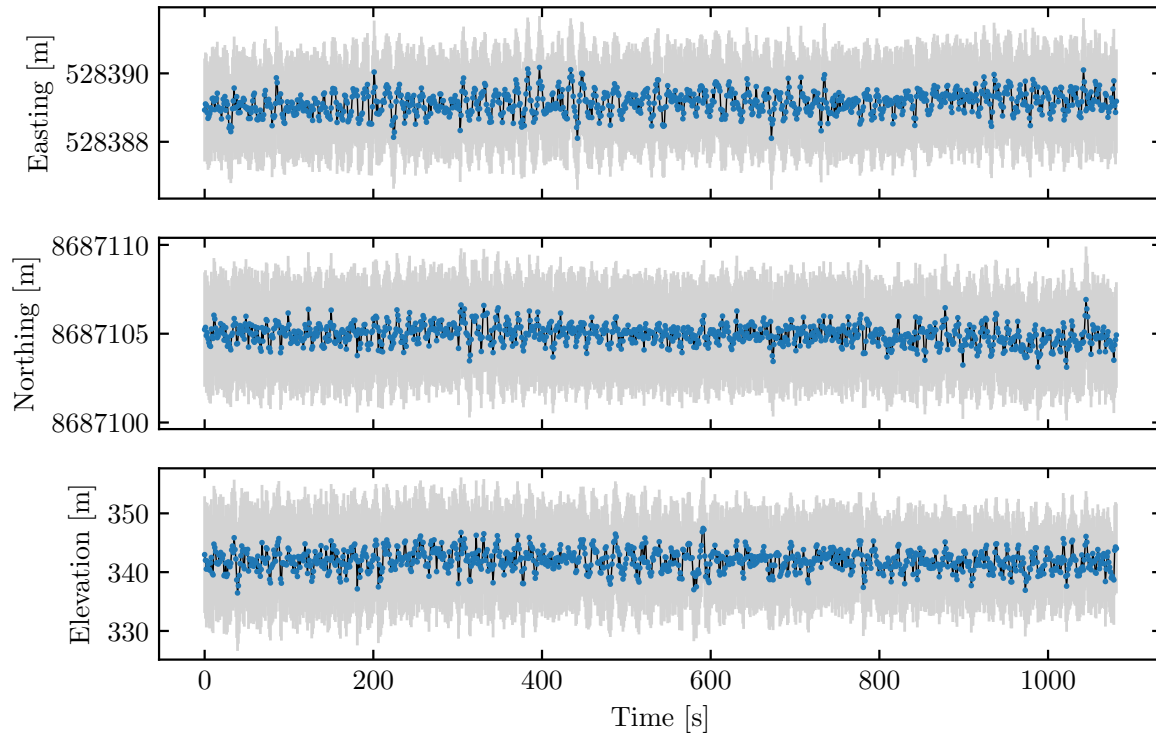


Figure 1.3.: First of two measurements of position of stake T1-2017 without the correction by the base station data. The blue points are the open source values Northing, Easting and Elevation in m in respect to the measurement time in s. The solid black line connect the data points. The gray shadowed range shows the uncertainty area.

To show the behaviour of the OS processed results it is useful to compare timeseries of the post processed position values for two measurements at the same stake on different days. In the first measurement (see Figure 1.4) the values converge after a few seconds to a fixed solution. In the second measurement (see Figure 1.5) the values vary during the time series without any tendency. The properties of the second measurement leads to a bigger difference between the TBC value and the OS value. A comparison to the whole time series of the TBC post processing is not possible, because this software do not provide the ability to have alternative outputs.

21-24

4 notes:

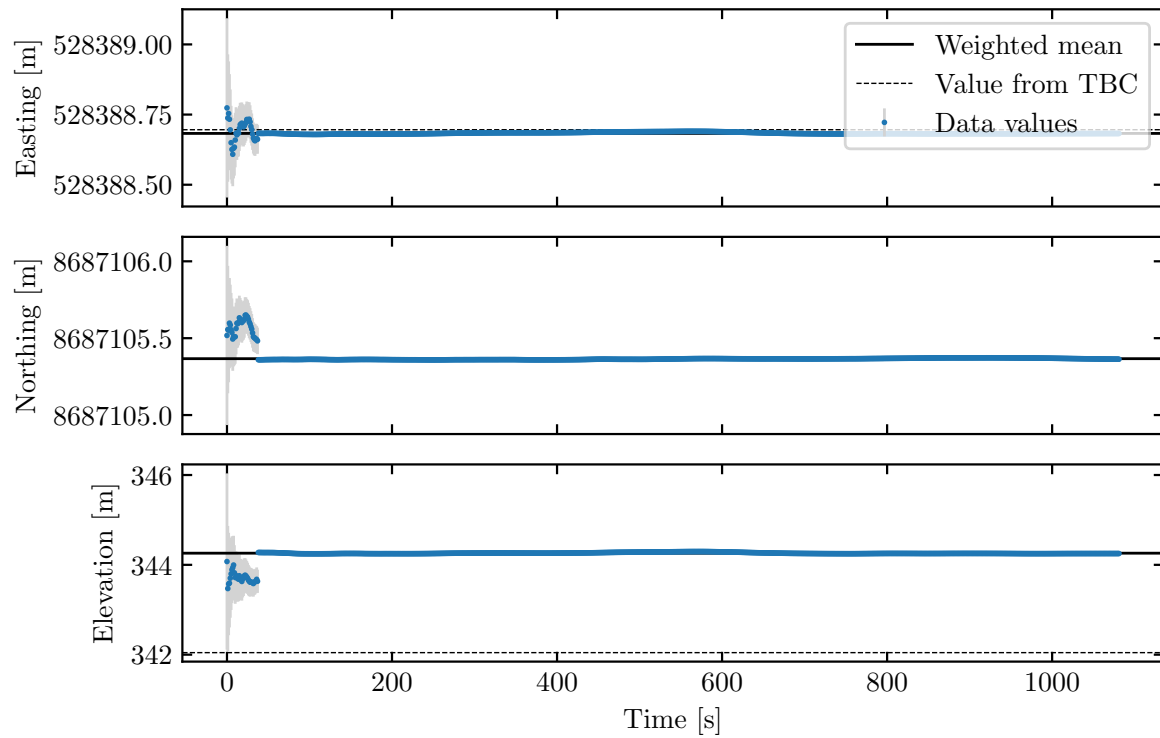


Figure 1.4.: First of two measurements of position of stake T1-2017 after the open source processing. The blue points are the open source values Northing, Easting and Elevation in m in respect to the measurement time in s. The solid black line is the weighted mean of the open source values. The dashed line is the Trimble Business Center value for the same stake. The gray shadowed range shows the uncertainty area.

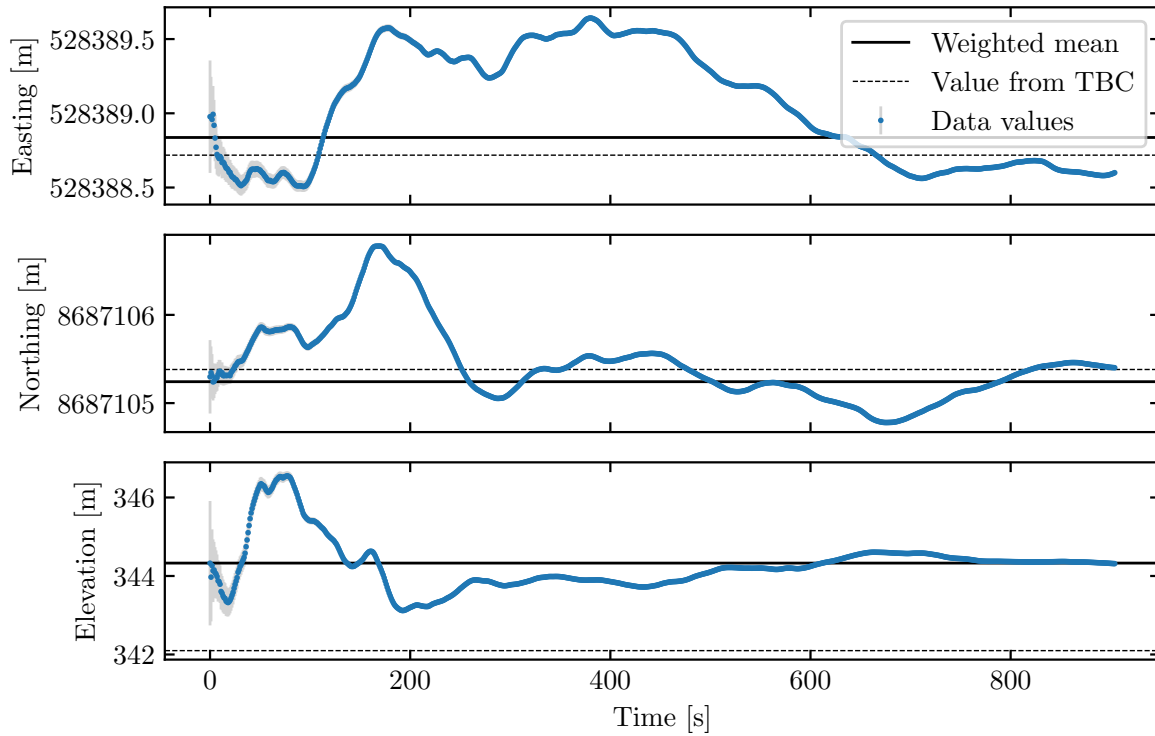


Figure 1.5.: Second measurement of two measurements of position of stake T1-2017 after the open source processing. The blue points are the open source values Northing, Easting and Elevation in m in respect to the measurement time in s. The solid black line is the weighted mean of the open source values. The dashed line is the Trimble Business Center value for the same stake. The gray shadowed range shows the uncertainty area.

1.4.3. Stake correction

The post processed data with the base station data are not the final position data. Finally, the differences due to the measurement setup has to be considered. For this a stake correction of every measurement includes the different aspects from our measurement setup (see 1.3.2). The distance between the rover and the stake has to be subtracted from the northing component. Also it was necessary to correct the position on the ice surface with the inclination of the stake. For this, we consider the inclination of the stake and calculate the error dependent on the height of the stake and the direction of the inclination. The measurement data which are relevant for our stake corrections are in the appendix in the A.1. For the better understanding all variables for the stake corrections are shown in the schematic figure 1.6. The formulas for the stake correction are derived by the geometry of our measurement setup.

25-26

2 notes:

27-28

2 notes:

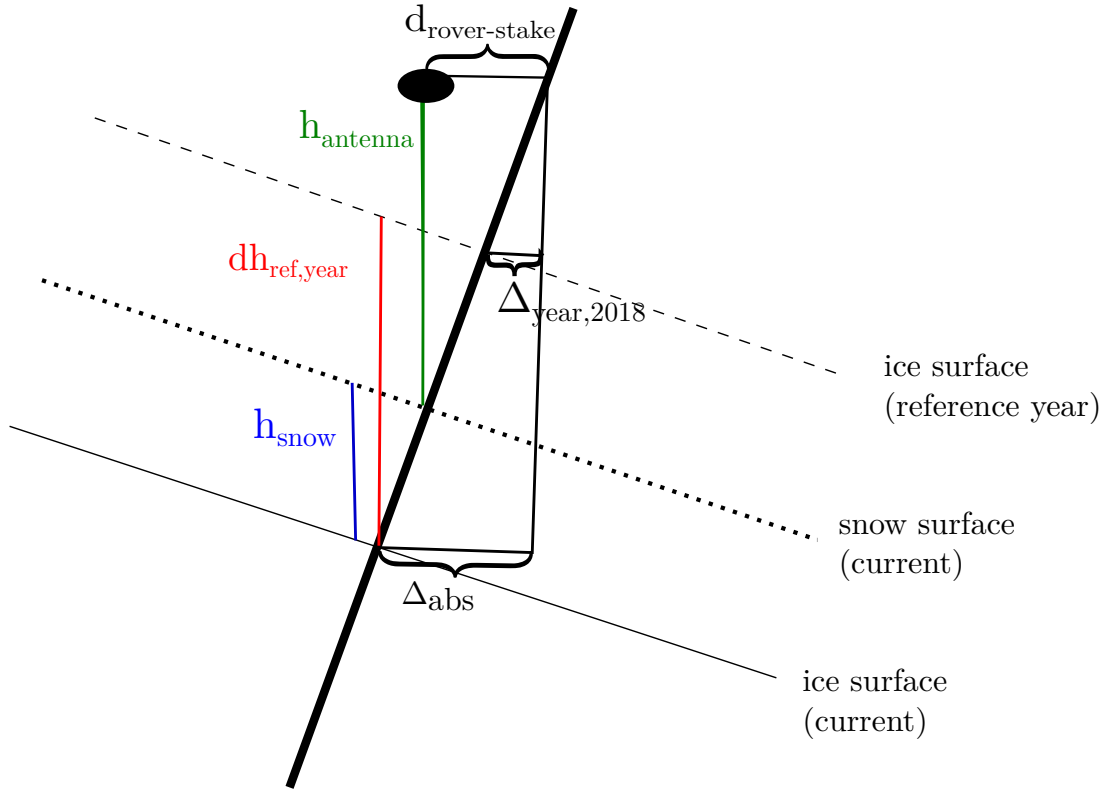


Figure 1.6.: Schematic figure with the setup and the relevant parameter for the stake correction and velocity calculation. The thick tilted line is the mass balance stake and the oval object is the rover. The dashed line shows the ice surface for the referenced year. The dotted line shows the snow surface and the solid line the ice surface of this year. The colored distances are the snow height h_{snow} (blue), antenna height h_{antenna} (green) and the ice surface height difference to the referenced year (red). Also the distance between rover and stake $d_{\text{year},2018}$ and the calculated absolute horizontal difference Δ_{abs} as well as the absolute horizontal absolute difference to the referenced year $\Delta_{\text{year},2018}$ are displayed in the scheme.

First the absolute horizontal difference Δ_{abs} depending in the inclination α and the height composite of snow depth h_{snow} and antenna height h_{antenna} .

$$\Delta_{\text{abs}} = (h_{\text{snow}} + h_{\text{antenna}}) * \sin(\alpha) \quad (1.20)$$

Then the correction is different for the northing and easting. The northing correction is calculated with the cosine of the direction of the inclination ϕ . The angle of direction is defined in a range from 0° to 359° with 0° for North, 90° for East, 180° for South and 270° for West. Due to geometrical reasons the sign has to be negative. Additionally, the distance between the rover and the stake $d_{\text{rover-stake}}$ has to be subtracted from the original northing.

$$\Delta_{\text{north}} = -(\Delta_{\text{abs}} * \cos(\phi)) - d_{\text{rover-stake}} \quad (1.21)$$

The easting difference Δ_{east} is calculated with the sine of ϕ .

$$\Delta_{\text{east}} = -\Delta_{\text{abs}} * \sin(\phi) \quad (1.22)$$

The elevation correction is different between the OS and the TBC values. For the TBC values the elevation correction $\Delta_{\text{elev,TBC}}$ only the h_{snow} need to be subtracted, because the h_{antenna} is already calculated out while the measurement with the Controller.

$$\Delta_{\text{elev,TBC}} = -h_{\text{snow}} \quad (1.23)$$

The elevation correction of the OS elevation $\Delta_{\text{elev,os}}$ is done by h_{snow} and h_{antenna} .

$$\Delta_{\text{elev,os}} = -(h_{\text{snow}} + h_{\text{antenna}}) \quad (1.24)$$

Referenced positions

To calculate the actual velocity it is necessary to reference the location of the stake to the ice surface elevation of the referenced year. This has been done for the years 2015, 2016 and 2017 on the 2018 OS values. The height for stake correction relating to the inclination is different, because the relevant height difference is changed by the height difference between this year and the referenced year $dh_{\text{year},2018}$. So this variable is considered for the calculation of the absolute horizontal difference $\Delta_{\text{year},2018}$. With this changed parameter the calculation works in the similar way.

$$\Delta_{\text{year},2018} = (h_{\text{snow}} + h_{\text{antenna}} - dh_{\text{year},2018}) * \sin(\alpha) \quad (1.25)$$

1.4.4. Evaluation

For the comparison to the OS post process the TBC post processed coordinates are given in the appendix in table A.2. The difference between the two different methods has no significant bias, which is proved by a small median (see table 1.1). The direction of the difference is randomly for between the stakes for all three parts of the positioning. The differences are mainly caused by a few big values after the post processing (compare table A.3). Due to this the mean value for the differences is higher than the median (see table 1.1)

Table 1.1.: Mean and median for the difference of northing, easting and elevation between the open source and Trimble Business Center values.

	Northing [m]	Easting [m]	Elevation [m]
mean difference	0.09	0.05	0.24
median of difference	0.01	0.01	0.09

1.4.5. Propagation of uncertainty

The calculations for the propagation of uncertainties are done by the common rule. The other uncertainties are determined by the quality of our measurements and first part of the processing (see table 1.2).

Table 1.2.: Used uncertainty values for the propagation of uncertainty with the uncertainty of inclination δ_α , direction of the inclination δ_ϕ , snow depth $\delta_{h_{snow}}$, antenna height $\delta_{h_{antenna}}$, ice surface height difference to the referenced year $\delta_{dh_{year,2018}}$, distance between rover and stake $\delta_{d_{rover-stake}}$ as well as the averaged uncertainties of the northing $\overline{\delta_N}$, easting $\overline{\delta_E}$ and elevation $\overline{\delta_H}$ after the open source post processing.

uncertainty	value
δ_α	3°
δ_ϕ	22.5°
$\delta_{h_{snow}}$	0.02 m
$\delta_{h_{antenna}}$	0.05 m
$\delta_{dh_{year,2018}}$	0.10 m
$\delta_{d_{rover-stake}}$	0.02 m
$\overline{\delta_N}$	0.40 m
$\overline{\delta_E}$	0.19 m
$\overline{\delta_H}$	0.89 m

The uncertainty of the absolute horizontal difference $\delta_{\Delta_{abs}}$ is dependent on the uncertainties of the parameter and the parameter itself.

$$\delta_{\Delta_{abs}} = \sqrt{(h_{snow} + h_{antenna})^2 * \delta_\alpha^2 * \cos^2(\alpha) + (\delta_{h_{snow}}^2 + \delta_{h_{antenna}}^2) * \sin^2(\alpha)} \quad (1.26)$$

The uncertainty of the northing correction $\delta_{\Delta_{north}}$ is

$$\delta_{\Delta_{north}} = \sqrt{\delta_{\Delta_{abs}}^2 * \cos^2(\phi) + \Delta_{abs}^2 * \delta_\phi^2 * \sin^2(\phi) + \delta_{d_{rover-stake}}^2} \quad (1.27)$$

The uncertainty of the easting correction $\delta_{\Delta_{east}}$ is

$$\delta_{\Delta_{east}} = \sqrt{\delta_{\Delta_{abs}}^2 * \sin^2(\phi) + \Delta_{abs}^2 * \delta_\phi^2 * \cos^2(\phi)} \quad (1.28)$$

The uncertainty of the elevation correction $\delta_{\Delta_{elev}}$ is

$$\delta_{\Delta_{elev}} = \sqrt{\delta_{h_{snow}}^2 + \delta_{h_{antenna}}^2} \quad (1.29)$$

The total uncertainty for northing $\delta_{\Delta_{total,north}}$, easting $\delta_{\Delta_{total,east}}$ and elevation $\delta_{\Delta_{total,elev}}$ incorporate the mentioned uncertainties $\delta_{\Delta_{north}}$, $\delta_{\Delta_{east}}$ and $\delta_{\Delta_{elev}}$ in addition to the uncertainties of the time series of the OS post processed GPS time series $\delta_{\Delta_{ts,north}}$ for northing, $\delta_{\Delta_{ts,east}}$ for easting and $\delta_{\Delta_{ts,elev}}$ for the elevation.

$$\delta_{\Delta_{total,north}} = \sqrt{\delta_{\Delta_{ts,north}}^2 + \delta_{\Delta_{north}}^2} \quad (1.30)$$

$$\delta_{\Delta_{total,east}} = \sqrt{\delta_{\Delta_{ts,east}}^2 + \delta_{\Delta_{east}}^2} \quad (1.31)$$

$$\delta_{\Delta_{\text{total,elev}}} = \sqrt{\delta_{\Delta_{\text{ts,elev}}}^2 + \delta_{\Delta_{\text{elev}}}^2} \quad (1.32)$$

The averaged uncertainties of the northing $\overline{\delta_N}$, easting $\overline{\delta_E}$ and elevation $\overline{\delta_H}$ (see table 1.2) are calculated from the total uncertainties.

Referenced positions

For the referenced positions only two equations differ to the previous uncertainty propagation due to the elevation. The uncertainty of the absolute difference $\Delta_{\text{year},2018}$ is

$$\begin{aligned} \delta_{\Delta_{\text{year},2018}} = & ((h_{\text{snow}} + h_{\text{antenna}} - dh_{\text{year},2018})^2 * \delta_{\alpha}^2 * \cos^2(\alpha) \\ & + (\delta_{h_{\text{snow}}}^2 + \delta_{h_{\text{antenna}}}^2 + \delta_{dh_{\text{year},2018}}^2) * \sin^2(\alpha))^{1/2} \end{aligned} \quad (1.33)$$

The uncertainty for the elevation correction $\delta_{\Delta_{\text{year,elev}}}$ is also different by the uncertainty of the height difference of the ice surface $\delta_{dh_{\text{year},2018}}$.

$$\delta_{\Delta_{\text{year,elev}}} = \sqrt{\delta_{h_{\text{snow}}}^2 + \delta_{h_{\text{antenna}}}^2 + \delta_{dh_{\text{year},2018}}^2} \quad (1.34)$$

1.4.6. Final positions

The final positions are based on the OS post processing and stake correction. This position values describe the position on the elevation of the ice surface. The corresponding uncertainties for each value are determined by the calculation of uncertainties (eq. 1.30 - 1.32). This values and uncertainties in table 1.3 are used in the next section to determine the velocities at the different stake locations. The referenced position can be calculated with the modified stake correction correction and error propagation on the OS post processed positions.

Table 1.3.: Final positions with Northing, Easting and Elevation for every stake after the open source post processing and stake correction with the corresponding error. The naming '-i' and '-ii' characterize the first and the second measurement at the same mass balance stake.

Name	Northing [m]	Easting [m]	Elevation [m]
BL2-2016	8686150.74 \pm 0.16	523049.41 \pm 0.11	436.89 \pm 0.48
BL2-2018	8686149.82 \pm 0.02	523051.47 \pm 0.03	437.74 \pm 0.06
BL3-2016	8686091.51 \pm 0.27	523544.75 \pm 0.13	490.82 \pm 0.25
BL3-2018	8686091.17 \pm 0.42	523545.34 \pm 0.10	491.39 \pm 1.03
BL4-2018	8686098.89 \pm 0.21	524181.02 \pm 0.20	570.94 \pm 0.20
BL4-i-2016	8686098.47 \pm 0.27	524179.80 \pm 0.19	571.65 \pm 0.20
BL4-ii-2016	8686098.39 \pm 1.30	524179.92 \pm 0.31	571.36 \pm 4.82
BL5-i-2017	8686130.74 \pm 0.09	524644.27 \pm 0.01	628.63 \pm 0.09
BL5-ii-2017	8686130.74 \pm 0.28	524644.28 \pm 0.15	628.56 \pm 0.75
T1-2018	8687106.55 \pm 0.32	528388.42 \pm 0.07	341.59 \pm 0.24
T1-i-2017	8687105.69 \pm 0.13	528388.68 \pm 0.18	341.26 \pm 0.12
T1-ii-2017	8687105.58 \pm 0.45	528388.84 \pm 0.44	341.38 \pm 0.65
T2-2016	8687321.31 \pm 0.42	527951.88 \pm 0.14	394.88 \pm 2.34
T2-2018	8687319.62 \pm 0.28	527951.35 \pm 0.27	395.86 \pm 1.61
T2-i-2017	8687321.37 \pm 0.30	527950.58 \pm 0.25	395.22 \pm 0.34
T2-ii-2017	8687320.98 \pm 1.31	527951.01 \pm 0.26	394.74 \pm 1.26
T3-2017	8687273.11 \pm 0.12	527598.29 \pm 0.01	422.59 \pm 0.07
T4-2016	8687138.56 \pm 0.47	527123.97 \pm 0.34	486.80 \pm 1.07
T4-2018	8687137.72 \pm 1.05	527124.90 \pm 0.37	487.94 \pm 2.33
T5-2016	8686938.28 \pm 0.57	526692.25 \pm 0.25	534.57 \pm 0.72
T5-2018	8686937.68 \pm 0.21	526690.76 \pm 0.21	535.09 \pm 0.45
T6-2016	8686675.01 \pm 0.51	526250.17 \pm 0.22	561.87 \pm 0.89
T6-2018	8686674.78 \pm 0.48	526246.88 \pm 0.39	560.47 \pm 0.79
T7-2015	8686580.26 \pm 0.26	525857.56 \pm 0.26	613.96 \pm 0.71
T7-2017	8686579.37 \pm 0.19	525858.38 \pm 0.04	615.95 \pm 0.71
T8-2017	8686471.52 \pm 0.48	525523.82 \pm 0.13	649.73 \pm 1.02

1.5. Results

1.5.1. Horizontal velocity (ice flow)

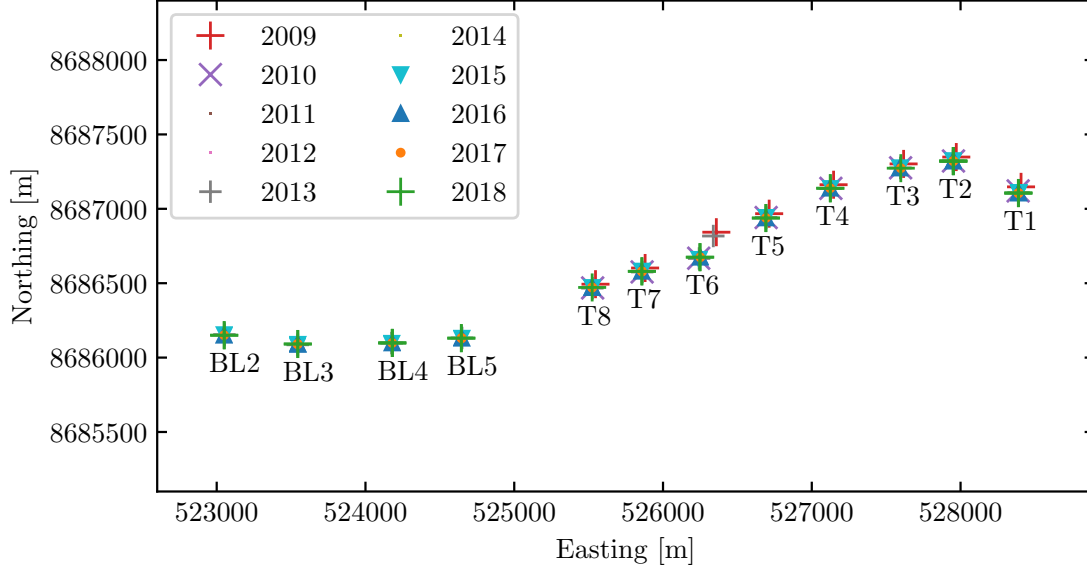


Figure 1.7.: Positions of all stakes in the flow line on Blekumbreen and Tellbreen. The different markers distinguish the year of the measurement.

Figure 1.7 shows the positions of the currently 12 different stake locations on Blekumbreen and Tellbreen. At those locations, a total of 26 measurements has been performed in 2018. Additionally, all available data of the stake positions since 2009 is shown on the figure. The coarse resolution of the figure shows a rough accordance of all of this years positions with the values of the last years. The stakes spread over about 5 kilometers in east-west direction and 1.5 kilometers in north-south direction.

Figure 1.8 shows all available data for one single stake (T1) in a higher resolution. The measurement of the location of T1-2017 (green) has been performed two times (Figs. 1.4 and 1.5) in order to estimate the uncertainty of the position. The two positions differ by 19 cm and match within their uncertainties.

Equation 1.35 gives the relation how the ice velocity v_{year} has been calculated from the corrected stake positions in Tab. 1.3: The distance between this years position and the position measured in 2017, 2016 or 2015 has been divided by the passed time t (1, 2 or 3 years). N_{year} and E_{year} are the northing and easting of the year which has been used to calculate the distance to this years position. The positions of this year ($N_{year,2018}$ and $E_{year,2018}$) have been shifted by the respective distance $\Delta_{ref,year}$ that ablation has added to inclined stakes since the year $year$, as described in section 1.4. Equation 1.36 shows how the error on v_{year} has been obtained. For the uncertainties on the past years values ($\delta_{N_{year}}^2$ and $\delta_{E_{year}}^2$), the mean uncertainties $\overline{\delta_N}$ and $\overline{\delta_E}$ of this years values from Tab 1.2 have been used.

Table 1.4 lists the calculated velocities for all stakes. The direction of the movements can be seen on the detailed figures for each stake in the appendix.

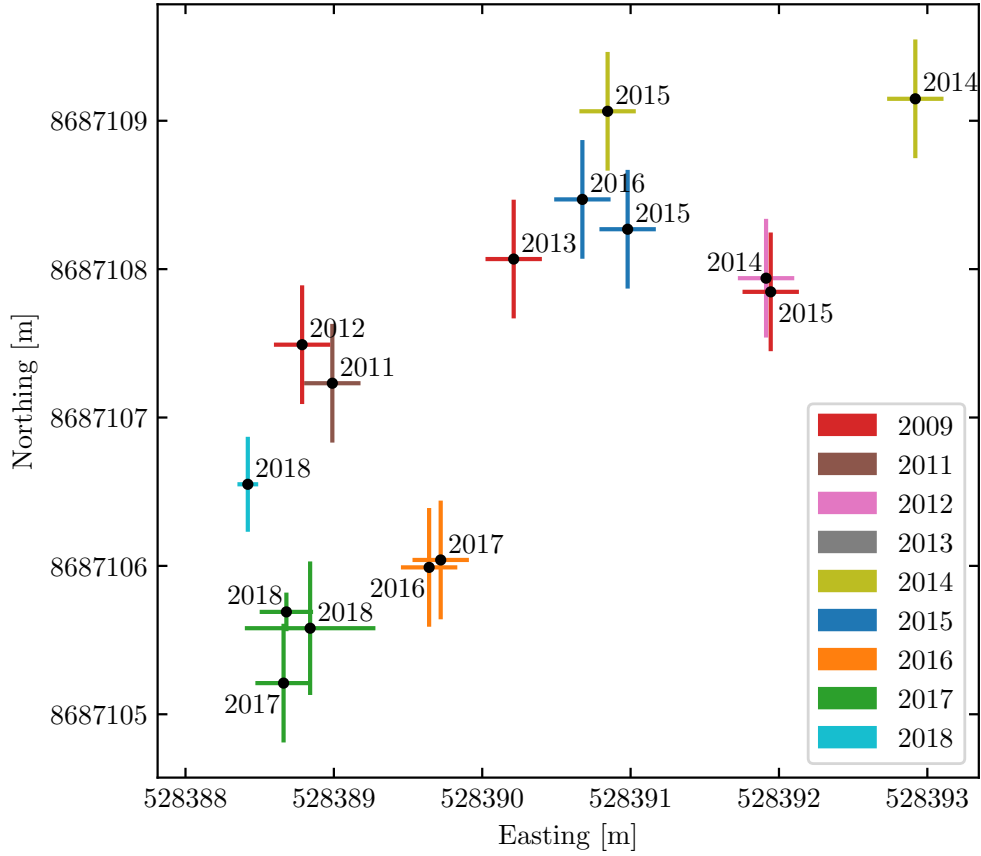


Figure 1.8.: Measured positions at the location of stake T1 from 2011 to 2018. Different colors denote different stakes; the year next to each stake position is the year of the measurement. The measurements of 2018 have been corrected by the inclination of the stake and the distance between the stake and the rover, therefore the coordinates refer to the intersection point of stake and glacier surface. At this location, a movement in south-east direction would be expected. This is not identifiable using the data at hand. Similar plots of the other 11 stake locations are situated in the appendix.

Table 1.4.: Velocities of the stakes measured in 2018, calculated with equations 1.35 and 1.36. The velocity v_{2017} has been calculated using last year's position. For inclined stakes, this position has been corrected for the horizontal displacement due to ablation. If available, corrected positions from 2016 and 2015 have also been used to obtain v_{2016} and v_{2015} . To be able to assess the uncertainty of the velocities, for measurements have been performed twice. This is denoted by the stakes -i and -ii.

Stake name	Velocity v_{2017} [m/a]	Velocity v_{2016} [m/a]	Velocity v_{2015} [m/a]
BL2-2016	0.26 ± 0.21	0.21 ± 0.19	-
BL3-2016	0.16 ± 0.20	0.21 ± 0.19	-
BL4-i-2016	0.07 ± 0.26	0.08 ± 0.25	-
BL4-ii-2016	0.11 ± 0.56	0.05 ± 0.48	-
BL5-i-2017	1.75 ± 0.18	-	-
BL5-ii-2017	1.74 ± 0.24	-	-
T1-i-2017	0.09 ± 0.10	-	-
T1-ii-2017	0.19 ± 0.43	-	-
T2-2016	0.60 ± 0.24	0.28 ± 0.20	-
T2-i-2017	0.23 ± 0.30	-	-
T2-ii-2017	0.53 ± 0.51	-	-
T3-2017	0.10 ± 0.11	-	-
T4-2016	0.13 ± 0.38	0.17 ± 0.37	-
T5-2016	0.30 ± 0.33	0.12 ± 0.22	-
T6-2016	0.79 ± 0.31	0.12 ± 0.19	-
T7-2015	0.26 ± 0.28	0.10 ± 0.15	0.08 ± 0.19
T7-2017	1.33 ± 0.16	-	-
T8-2017	0.20 ± 0.24	-	-

$$v_{year} = \frac{\sqrt{(N_{year,2018} - N_{year})^2 + (E_{year,2018} - E_{year})^2}}{t} \quad (1.35)$$

$$\delta_{v_{year}} = \sqrt{\frac{(\delta_{N_{year,2018}}^2 + \delta_{N_{year}}^2) * (N_{year,2018} - N_{year})^2 + (\delta_{E_{year,2018}}^2 + \delta_{E_{year}}^2) * (E_{year,2018} - E_{year})^2}{(N_{year,2018} - N_{year})^2 + (E_{year,2018} - E_{year})^2}} \quad (1.36)$$



1.5.2. Vertical velocity (mass balance)

Besides the horizontal position, the GPS data also contain elevation. An analysis of the change of elevation (the vertical velocity) of the stakes over the past years offers the possibility to determine the individual average mass balances.

We have been able to find elevation data from former groups for the last 7 years, back until 2011. Figures 1.9 and 1.10 show this data, together with the new data from 2018. For most of the old data points, the uncertainties are not known. Therefore there are no error bars shown on the plots.

38-39

2 notes:

Apart from a couple of outliers, the elevation of all stakes decreases quite   far. Therefore linear fits of the elevation have been performed for all stakes individually. The results of the fits are shown in Tables 1.5 and 1.6.

With the individual mass balances for each stake, it is possible to calculate the mass balance gradients and the equilibrium line elevations of the two glaciers. This is shown in Figs. 1.11 and 1.12. The values on the y-axis (stake elevation) are mean values of all elevation measurements of the different years.

The linear fits yield the following results for the equilibrium lines (EL) and mass balance gradients (MBG) on Blekumbreen and Tellbreen:

$$\begin{aligned} \text{EL}_B &= 751 \pm 45 \text{ m} & \text{MBG}_B &= 5.1 \pm 1.0 \text{ mm/m} \\ \text{EL}_T &= 757 \pm 56 \text{ m} & \text{MBG}_T &= 6.8 \pm 1.4 \text{ mm/m} \end{aligned}$$

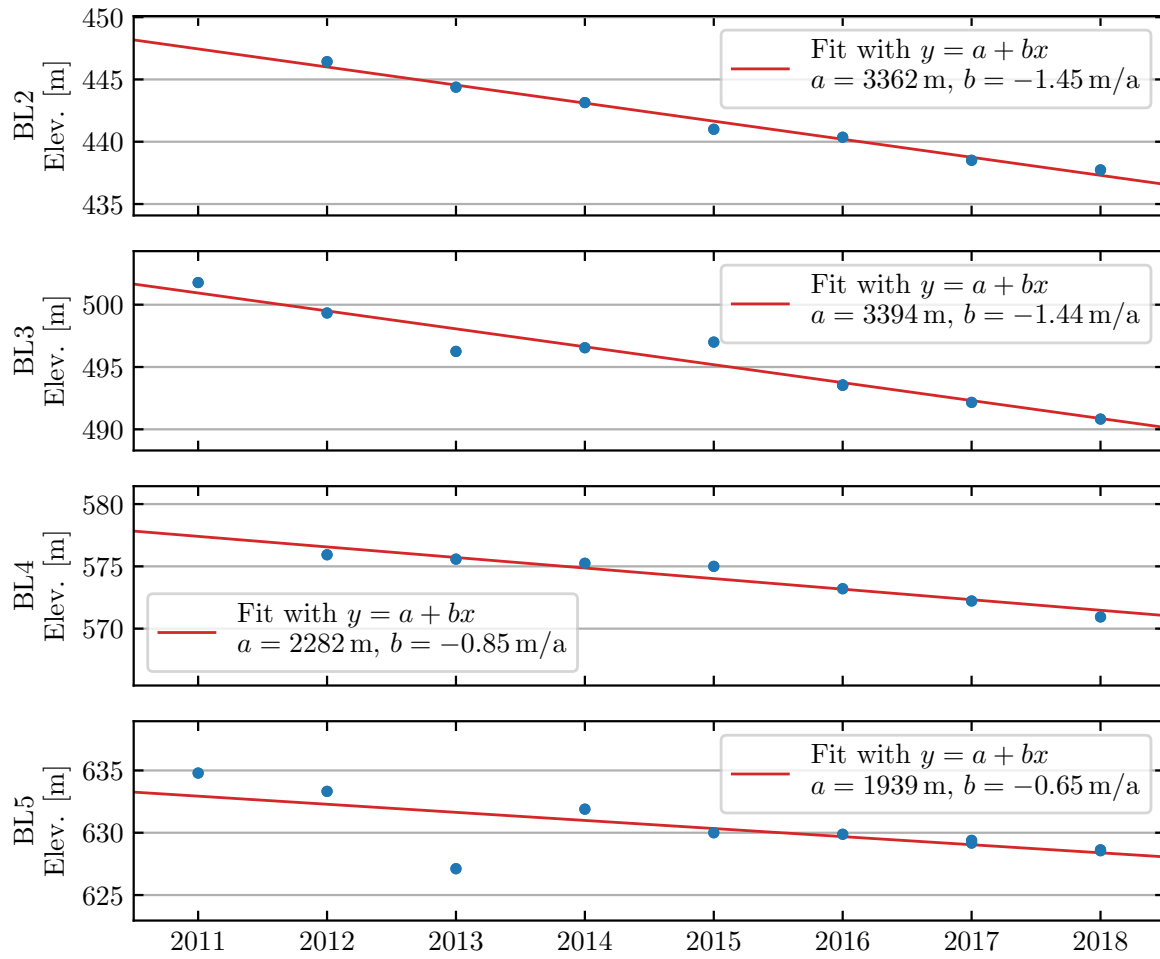


Figure 1.9.: GPS measured elevation of the stakes on Blekumbreen from 2011 until 2018 (blue dots). Linear fits (red line) of the data have been performed to calculate the individual mass balances b .

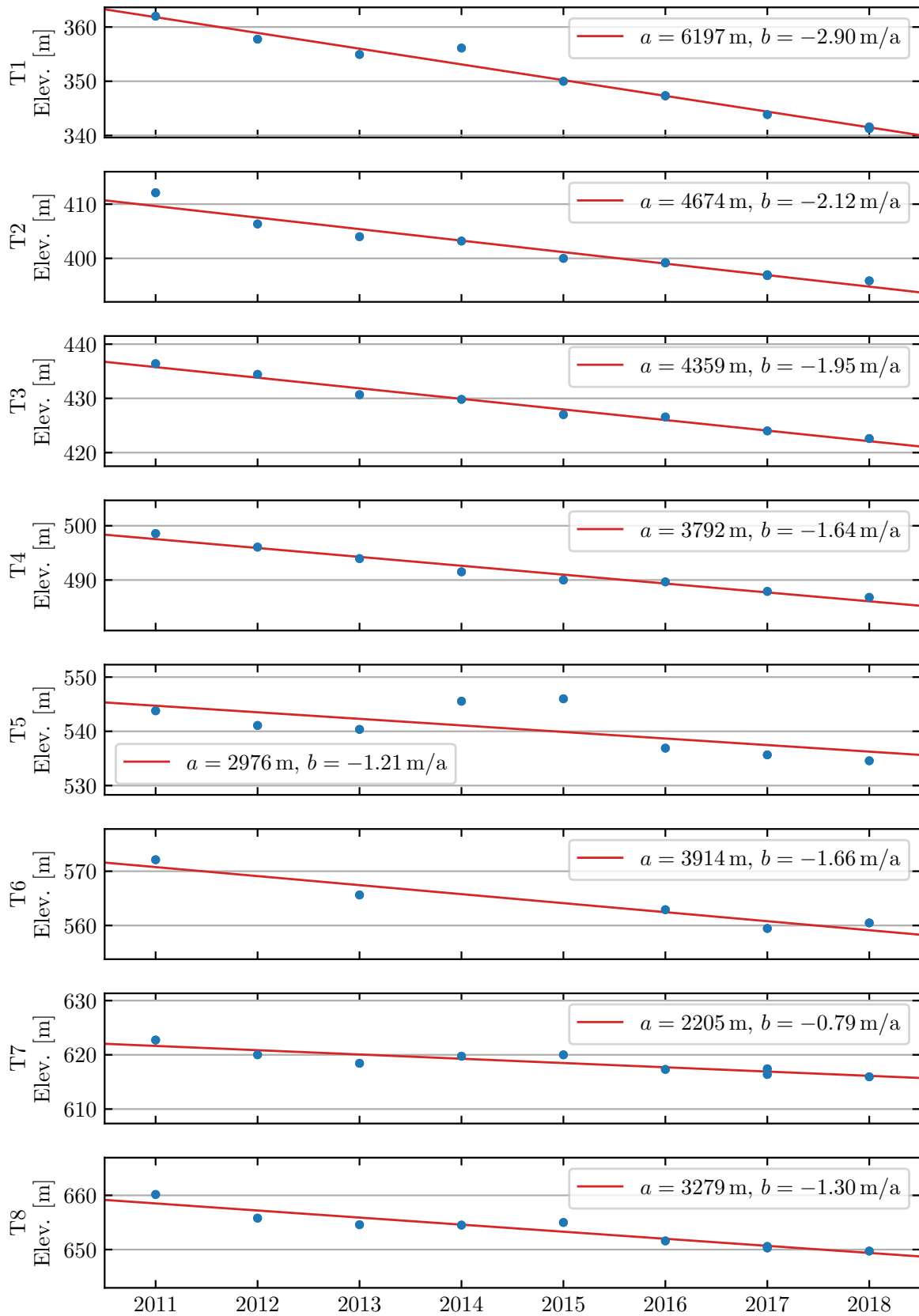


Figure 1.10.: GPS measured elevation of the stakes on Tellbreen from 2011 until 2018 (blue dots). Linear fits (red line) with $y = a + x * b$ have been performed to calculate the individual mass balances b .

Table 1.5.: Mass balance as result of the elevation fits from Fig. 1.9 and mean values of the elevation measurements for all stakes on Blekumbreen. The data in the table is plotted in Fig. 1.11.

Stake name	Elevation [m]	Mass balance [m]
BL2	441.7	-1.45 ± 0.08
BL3	495.7	-1.44 ± 0.16
BL4	574.0	-0.85 ± 0.11
BL5	630.3	-0.65 ± 0.24

Table 1.6.: Mass balance as result of the elevation fits from Fig. 1.10 and mean values of the elevation measurements for all stakes on Tellbreen. The data in the table is plotted in Fig. 1.12.

Stake name	Elevation [m]	Mass balance [m]
T1	349.4	-2.90 ± 0.15
T2	401.4	-2.12 ± 0.17
T3	428.9	-1.95 ± 0.12
T4	491.8	-1.64 ± 0.13
T5	540.5	-1.21 ± 0.55
T6	564.1	-1.66 ± 0.30
T7	618.7	-0.79 ± 0.15
T8	653.6	-1.30 ± 0.17

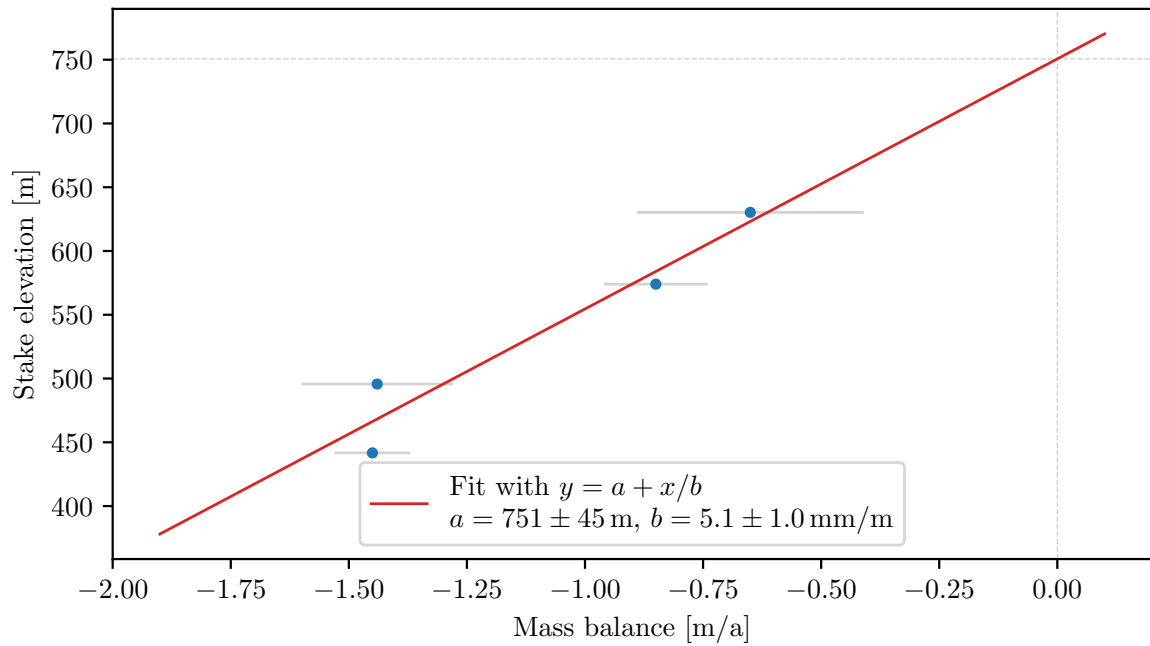


Figure 1.11.: Mass balances of the stakes on Blekumbreen as a function of stake elevation and linear fit of the points to obtain the equilibrium line elevation a and the mass balance gradient b .

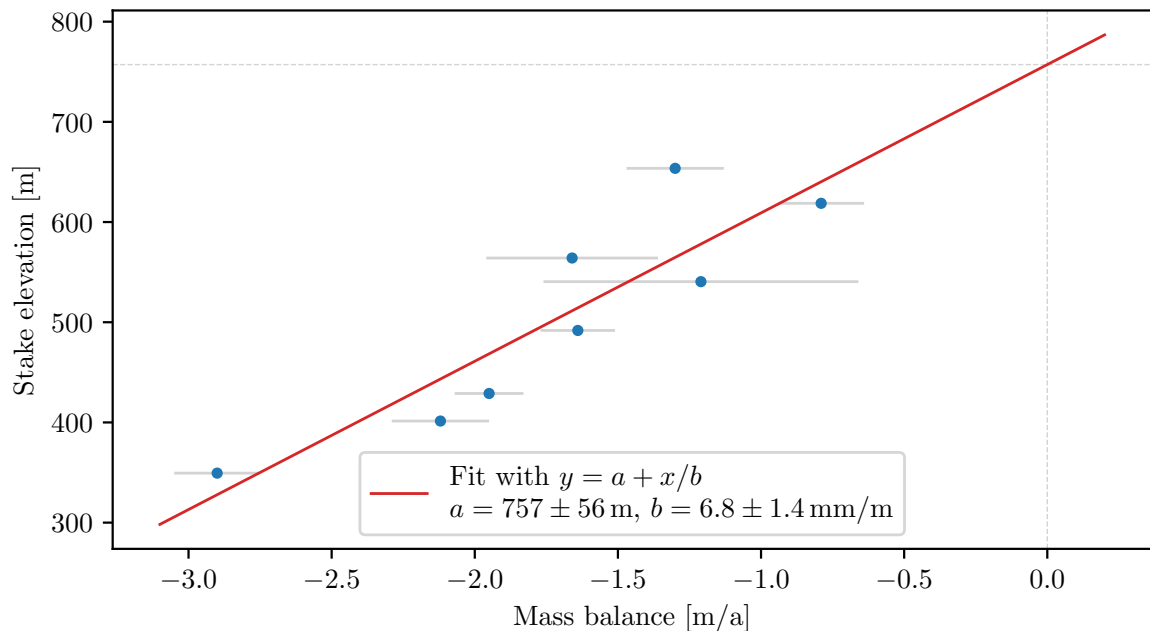


Figure 1.12.: Mass balances of the stakes on Tellbreen as a function of stake elevation and linear fit of the points to obtain the equilibrium line elevation a and the mass balance gradient b .

1.5.3. Theoretical surface velocity

Based on the shallow ice approximation it is possible to calculate a theoretical surface velocity for the glaciers we did our measurements on. To make the calculation (see 1.12) the variables slope angle, ice velocity and ice thickness has to be chosen. The ice density is assumed as 917 kg/m^3 and the gravitational acceleration as 9.81 m/s^2 . The values for the ice viscosity are displayed in table 1.7. It is not possible to determine the exact ice temperature. Because of this, the calculation is done for viscosities for different ice temperatures T .

Temperature [°C]	0	-5	-10	-15
Ice viscosity [P/a^{-3}]	$5,52 \cdot 10^7$	$8,63 \cdot 10^7$	$1.28 \cdot 10^8$	$1.52 \cdot 10^8$

Table 1.7.: Ice viscosities for different ice temperatures $T = \{0, -5, -10, -15\}$

The theoretical velocity is mainly influenced by the ice thickness (see tables 1.8, 1.9 and 1.10). For the mean thickness the theoretical surface velocity of ice has the order of magnitude of centimeters. The small velocity value corresponds with the measured velocities (compare 1.4).

Table 1.8.: Theoretical surface velocity u_{\odot} [m/a], $\alpha = 5$

$\alpha = 5$	$H_{min} = 1$	$H_{avg} = 33.4$	$H_{max} = 82.3$
B($T = 0 \text{ C}$)	$4.51 \cdot 10^{-8}$	$5.61 \cdot 10^{-2}$	2.07
B($T = -5 \text{ C}$)	$1.18 \cdot 10^{-8}$	$1.47 \cdot 10^{-2}$	$5.43 \cdot 10^{-1}$
B($T = -10 \text{ C}$)	$3.63 \cdot 10^{-9}$	$4.51 \cdot 10^{-3}$	$1.17 \cdot 10^{-1}$
B($T = -15 \text{ C}$)	$2.17 \cdot 10^{-9}$	$2.71 \cdot 10^{-3}$	$9.98 \cdot 10^{-2}$

Table 1.9.: Theoretical surface velocity u_{\odot} [m/a], $\alpha = 6$

$\alpha = 6$	$H_{min} = 1$	$H_{avg} = 33.4$	$H_{max} = 82.3$
B($T = 0 \text{ C}$)	$7.78 \cdot 10^{-8}$	$9.68 \cdot 10^{-2}$	3.57
B($T = -5 \text{ C}$)	$2.04 \cdot 10^{-8}$	$2.54 \cdot 10^{-2}$	$9.37 \cdot 10^{-1}$
B($T = -10 \text{ C}$)	$6.26 \cdot 10^{-9}$	$7.79 \cdot 10^{-3}$	$2.87 \cdot 10^{-1}$
B($T = -15 \text{ C}$)	$3.75 \cdot 10^{-9}$	$4.67 \cdot 10^{-3}$	$1.72 \cdot 10^{-1}$

Table 1.10.: Theoretical surface velocity u_{\odot} [m/a], $\alpha = 7$

$\alpha = 7$	$H_{min} = 1$	$H_{avg} = 33.4$	$H_{max} = 82.3$
B($T = 0 \text{ C}$)	$1.23 \cdot 10^{-7}$	$1.53 \cdot 10^{-1}$	5.66
B($T = -5 \text{ C}$)	$3.24 \cdot 10^{-8}$	$4.03 \cdot 10^{-2}$	1.49
B($T = -10 \text{ C}$)	$9.92 \cdot 10^{-9}$	$1.23 \cdot 10^{-2}$	$4.55 \cdot 10^{-1}$
B($T = -15 \text{ C}$)	$5.95 \cdot 10^{-9}$	$7.40 \cdot 10^{-3}$	$2.73 \cdot 10^{-1}$

The theoretical calculation can be applied on the different stake locations. The surface velocity for the ice temperature of -5°C and -10°C are comparable results to the measurement values (see table 1.11). Also the theoretical calculated mass balance confirm with overall negative values that both glaciers are completely in the ablation zone (see subsec. 1.5.2).

Table 1.11.: Theoretical surface velocity at all the stakes. "no data" translates into an absence of data for the Ice Thickness

Stake	Northing [m]	Easting [m]	Ice Thickness [m]	$u_{\odot}^{T=-5} [m/a]$	$u_{\odot}^{T=-10} [m/a]$	Mass balance [m/a]
BL2-2018	8686150	523051	66.48	0.40	0.12	-1.1475
BL3-2018	8686091	523545	53.46	0.17	0.05	-0.9095
BL4-2018	8686099	524181	34.96	0.03	0.01	-0.6885
BL5-2017	8686131	524644	75.92	0.68	0.21	-0.119
T1-2018	8687107	528388	no data	-	-	-2.108
T2-2018	8687320	527951	no data	-	-	-1.42375
T3-2017	8687273	527598	no data	-	-	-1.1985
T4-2018	8687138	527125	47.09	0.10	0.03	-0.731
T5-2018	8686938	526691	61.97	0.30	0.09	-0.646
T6-2018	8686675	526247	69.80	0.48	0.15	-0.323
T7-2017	8686579	525858	55.68	0.20	0.06	-0.221
T8-2017	8686472	525524	27.28	0.01	0.00	-0.5525

1.6. Discussion

1.6.1. Horizontal velocity

As the two glaciers move down the slope of the mountains, we expect an eastward stake movement on Tellbreen and a westward movement on Blekumbreen, with not too much variation of the velocity over the years. For many of the stakes, this is not the case. The movement is sometimes perpendicular to the flow line of the glaciers and at times even uphill. In the past years, this has been explained by a 'local squeeze and stretch movement' (Hein and Zeigermann, 2016) or the 'shrinking and swelling of a melt water channel' (Schoonhoven and Demane, 2017). Although those explanations may be true, we see no clear evidence of a horizontal glacier movement in the measurement data. From the 18 stake velocities v_{2017} which were calculated (Tab. 1.4), eleven velocities include a velocity of zero within their uncertainty. Some of the seven remaining velocities which are far from zero could be explained with outliers due to unknown reasons, e.g. issues with the stake position of last year or a failure of the post processing algorithm.

In any case, a Gaussian distribution of the measured values implies that 32 % of the values do not include zero within their $1-\sigma$ interval, if the actual glacier velocity is zero. This corresponds to six out of 18 stakes. Looking at the velocity values in Tab. 1.4 this way, we can not reject the null hypothesis that the glaciers are not moving.

Nevertheless, a few stakes show some coherent movement. Therefore each of the stakes will subsequently shortly be discussed.

T1 The positions from 2009 until 2015 exhibit an intermittent eastward movement, which is in accordance to the flow line direction at this position (east to south-east). In 2015, the stake has moved about 2 m up the slope, which is implausible. The values of 2016 and 2017 coincide within their uncertainties and show no movement at all. 2018 the measurement of the position has been performed twice. The two positions agree to each other. The two new data points are north of the 2017 position, but considering the error bars, this direction is not significant.

T2 The measurements before 2017 show no stake movement. The two measurements of T2-2017 that have been conducted this year agree within their uncertainties and also not significantly away from the position of 2017. The older stake T2-2016 also did not move significantly.

T3 None of the four stakes show any significant movement.

T4 The measurements before 2015 show a slight northwards trend. This years position of T4-2016 lies between the positions of 2016 and 2017.

T5 The measurements before 2015 may have an intermittent north-eastwards trend. T5-2016 is has not been moving significantly for the last three years.

T6 Data from before 2015 are partly missing and this data show an unexpected jump of about 6 m southwards. The 2016 position of T6-2016 lies between the values of 2017 and 2018, but all three differ not significantly from each other.

T7 Positions before 2015 are inconsistent. The positions of T7-2015 lie all within their uncertainties since 2015. T7-2017 exhibits an unexpected movement to north west.

T8 For three out of four different stakes on location T8, all position measurements are indistinguishable due to uncertainty. The two measurements of T8-2015 differ slightly more, but not very significantly in the expected eastwards direction.

BL2 BL2-2011 shows a rather consistent westwards movement along the flow line of the glacier until 2015. The subsequently placed stake BL2-2016 continues this tendency until 2018. Therefore we can have some confidence in the calculated velocities $v_{2017} = 26 \pm 21$ cm/a and $v_{2016} = 21 \pm 19$ cm/a.

BL3 Also for BL3-2011, a westwards drift is visible. The measurement value of 2013 is obviously an outlier. BL3-2015 continues a north-west drift from 2015 until 2017. The 2018 value for the position of BL3-2016 does not continue the trend of the prior stakes. The positions of this stake from 2016 to 2018 are very close together.

BL4 Likewise for BL4-2011, a slight westwards drift with an outlier in 2013 is observed. The more recent position measurements of BL4-2016 are not distinguishable.

BL5 BL5-2011 has constantly been moving westwards for seven years, from 2011 until 2017. Surprisingly, this years position of BL5-2017 suggests a velocity as large as 1.75 ± 0.18 m/a and 1.74 ± 0.24 m/a (Tab. 1.4). As the position measurement has been conducted two times in 2018 and the obtained positions are almost the same, we suspect an error in the position measurement of 2017.

In summary, the analysis of the entire data set of the stake positions on Tellbreen seems to provide no evidence of a consistent glacier movement. Single events of stake movements in various directions could be explained by local and short-time displacements due to the forming of melt water channels or crevasses, like in the last reports. But looking at the bigger picture of all available data, we advance the view that a movement of Tellbreen is not detectable with the applied measurement method, and that individual apparent stake movements are caused by the uncertainty of the method. This view is supported by a comparison with the theoretical values for the glacier velocity. As the measurements provide no reliable value for the glacier velocity, a reasonable calculation of the ice flow volume can not be made.

On Blekumbreen, the situation is different. The investigation of the seven year long time series since 2011 makes a trend visible, which could hardly be discovered by comparing positions of only two consecutive years. Even though the uncertainties makes it impossible to show a movement of Blekumbreen with only this years and last years positions. Looking back longer in the past gives clear evidence of a small, but coherent movement along the flow line of Blekumbreen.

To improve the quality of the results, the main sources of uncertainty have to be identified. One large source is the GPS measurement itself. The surrounding mountains are covering a great part of the sky, thereby hiding a few satellites and probably prohibit a fixed solution in some measurements. Without a fixed solution the result can taken, but cannot be expected as an exact positioning. Reflections from the metal stake could deteriorate the signals and should be avoided. The distance to the base station on Platåbreen is relatively long and the time series of some measurements show, that the correction with the base station data can not fully remove artefacts, possibly due to atmospheric disturbances.

The second big error source is the inclination of some stakes. In conjunction with ablation, the inclination of the stake adds a displacement which has to be corrected. The therefore necessary measurement of angle and direction of inclination can only be performed with a high uncertainty. For example, a stake inclination of 10° together with an ablation of 1 m shifts the entry point of the stake into the ice by 17 cm. If this displacement is not corrected, it adds an error in the order of the annual displacement of the glacier.

Another source of error is that each years group employs slightly different proceedings in terms of the measurement setup and the data post processing.

An interesting result of the open source post processing is that the mean uncertainty on the northing is more than twice as large as on the easting (Tab. 1.2). The reason for this could be the location of Svalbard close to the north pole, which creates an asymmetric satellite geometry more suitable to measure easting than northing. Also the rover is in most of the measurements positioned northwards, which gives an addational error source due to the uncertainty of the measured distance between rover and stake.

1.6.2. Vertical velocity

The analysis of the vertical stake movement yields much more reliable results than for the horizontal velocity. Even though an analysis of the vertical component has already been performed twice (Hein and Zeigermann (2016) and Schoonhoven and Demane (2017)). We are the first group who could calculate the equilibrium line elevation and the mass balance gradient for both glaciers only from GPS data. The results are in good agreement with the findings of the mass balance group, who report equilibrium lines of 673 m for Tellbreen and 678 m for Blekumbreen as well as mass balance gradients of 5.7 mm w.e./m for Tellbreen and 5.3 mm w.e./m for Blekumbreen.

The individual mass balances of the stakes exhibit a linear behaviour for both glaciers. Only T8 and T6 on Tellbreen have a higher ablation than expected from the linear fit. This could be due to local variations of the terrain around the stakes, like local radiation or wind conditions.

Both equilibrium lines and mass balance gradients for Tellbreen and Blekumbreen coincide within their uncertainties. The equilibrium line elevations are about 100 m above the highest stake on Tellbreen, which means that there are no accumulation zones on the glaciers.

Even though measuring mass balance by GPS is a much coarser method than measuring it with a tape measure on stakes. We think that by considering a long time series of elevation measurements, it could eventually be even more precise, because statistical fluctuations of single years have less influence. Additionally, measurement errors of single years can easily be detected, because elevation values of not consecutive years can be compared. This is not possible with the usual method of measuring the mass balance with a ruler, when new stakes have to be placed.

1.7. Conclusion

The new open source post processing method provides similar results for the stake positions as the software TBC. Therefore the licensed TBC software can be replaced by the open source method.

Based on the results of the measured and theoretically calculated ice velocities we can confirm the low velocities measured in the last years. With the applied measurement method, we were not able to measure accurate flow velocities of Blekumbreen and Tellbreen. We can only specify upper limits for the velocity, which are the uncertainties of 0.40 m for northing and 0.19 m for easting. The theoretical surface velocity of the shallow ice approximation validates the small values for the horizontal velocity.

Due to a faster movement in the vertical direction, it is possible to calculate - even with an uncertainty of 0.89 m on the individual elevations - a vertical velocity. Thus we are able to calculate mass balances for both glaciers, which shows that the whole area of the glaciers is in the ablation zone.

With the findings in this report, we are able to propose improvements to the setup and the methods, which could eventually help to increase the accuracy of the collected coordinates and enable the precise measurement of the very small flow velocities of the glaciers.

We found it helpful to measure some stakes two times. If all stakes were measured two

times, a comparison of each two positions would offer a sound method of determining the uncertainties.

Even though we tried our best to correct the measurement data for the distance of the rover to the stake and the inclination of some stakes, the corrections did not reduce the uncertainties on the positions sufficiently. Therefore, our suggestion for the improvement is make sure that stakes are always drilled straight. We advise not to use inclined stakes at all for the velocity measurement, because the error added by the high ablation values is hardly controllable. Additionally, it would make the measuring procedure a lot simpler if the stake of the rover could be placed every time into the stake, instead of next to it. This could be achieved if the stakes are cut down to a reachable level every year when they have been melted out a lot.

Bibliography

- Churcher, B., 2011: Differential global positioning system.
- Gölles, T., 2012: Trimble GNSS quick-start manual. *University Center of Svalbard*.
- Hein, G., and Zeigermann, L., 2016: Glacier velocities and Ice Flux. *AGF-212, final report 2016*.
- Hooke, R. L., 2005: *Principles of Glacier Mechanics*. Cambridge.
- J. F. Nye, 1952: The Mechanics of Glacier Flow.
- J. W. Glen, 1955: The creep of polycrystalline ice.
- K. M. Cuffey, W. S. B. P., 2010: *The Physics of Glaciers*. Elsevier.
- Kaplan, E., and Hegarty, C., 2005: *Understanding GPS: principles and applications*. Artech house.
- Ralf Greve, H. B., 2009: *Dynamics of Ice Sheets and Glaciers*. Springer.
- Schoonhoven, D., and Demane, Y., 2017: Ice velocity and flux. *AGF-212, final report 2017*.
- Trimble Survey division, 2012: Trimble HD-GNSS processing.

Appendices

A. Appendix Ice velocity

Header of a position file

```
program      : RTKPOST ver.2.4.2
inp file     : *.obs
inp file     : lyrs07*0.18o
inp file     : *.nav
obs start    : 2018/03/11 14:22:12.0 GPST (week1992  51732.0s)
obs end      : 2018/03/11 14:37:48.0 GPST (week1992  52668.0s)
pos mode     : static
freqs        : L1+L2
solution     : forward
elev mask    : 15.0 deg
dynamics     : on
tidecorr     : off
ionos opt    : broadcast
tropo opt    : saastamoinen
ephemeris    : broadcast
navi sys     : gps glonass galileo qzss sbas
amb res      : fix and hold
amb glo      : on
val thres    : 3.0
antenna1     :                ( 0.0000  0.0000  0.0000)
antenna2     :                ( 0.0000  0.0000  0.0000)
ref pos      : 78.228825638    15.397310064    495.6816
```

Additional data in the processing

Table A.1.: Measurements of the setup parameter used for the stake correction.

Name	Date	Antenna height [m]	Snow depth [m]	Inclination [deg]	Direction of Incl. [deg]	Distance Rover-Stake [m]
BL2-2016	15.03.2018	2.18	1.1	3	225	0.18
BL2-2018	15.03.2018	0.6	0	2	270	0
BL3-2016	15.03.2018	2.2	1.07	12	270	0.1
BL3-2018	15.03.2018	0.6	0	0	0	0
BL4-2018	15.03.2018	0.92	0	0	0	0
BL4-i-2016	15.03.2018	2.08	0.93	10	270	0.11
BL4-ii-2016	16.03.2018	1.25	1.25	10	270	0.2
BL5-i-2017	15.03.2018	1.32	1.1	0	0	0
BL5-ii-2017	16.03.18	0.48	1.3	0	0	0
T1-2018	13.03.2018	0.66	0	0	0	0
T1-i-2017	11.03.2018	2.2	0.8	9	180	0.15
T1-ii-2017	13.03.2018	2.15	0.8	10	180	0.17
T2-2016	15.03.2018	1.34	0.97	0	0	0.1
T2-2018	13.03.2018	0.66	0	5	225	0
T2-i-2017	11.03.2018	2.23	1	10	90	0.1
T2-ii-2017	13.03.2018	1.4	1	5	135	0.1
T3-2017	11.03.2018	1.87	1.05	0	0	0.1
T4-2016	11.03.2018	2.42	1.2	5	0	0.1
T4-2018	13.03.2018	0.63	0	0	0	0
T5-2016	11.03.2018	2.44	1.22	8	0	0.1
T5-2018	15.03.2018	0.45	0	0	0	0
T6-2016	11.03.2018	2.3	1.35	4	180	0.15
T6-2018	15.03.2018	1.95	1.4	0	0	0
T7-2015	13.03.2018	1.84	1.2	10	45	0.1
T7-2017	13.03.2018	0.98	1.21	0	0	0
T8-2017	13.03.2018	2.09	0.7	5	180	0.1

Table A.2.: Final TBC positions in Northing, Easting and Elevation with stake correction.

Name	Northing [m]	Easting [m]	Elevation [m]
BL2-2016	8686150.73	523049.40	436.86
BL2-2018	8686149.81	523051.47	437.76
BL3-2016	8686091.55	523544.71	491.07
BL3-2018	8686091.13	523545.37	491.15
BL4-2018	8686098.89	524181.02	571.86
BL4-i-2016	8686098.48	524179.80	571.55
BL4-ii-2016	8686098.40	524179.93	571.36
BL5-i-2017	8686130.74	524644.30	628.64
BL5-ii-2017	8686130.74	524644.29	628.61
T1-2018	8687106.61	528388.32	341.43
T1-i-2017	8687105.68	528388.70	341.25
T1-ii-2017	8687105.72	528388.72	341.30
T2-2016	8687320.86	527951.55	395.12
T2-2018	8687319.48	527951.22	395.13
T2-i-2017	8687321.37	527950.59	395.17
T2-ii-2017	8687321.53	527951.08	395.25
T3-2017	8687273.10	527598.30	422.57
T4-2016	8687138.56	527123.96	486.78
T4-2018	8687137.40	527124.77	487.25
T5-2016	8686938.28	526692.26	534.57
T5-2018	8686937.70	526690.76	535.26
T6-2016	8686675.02	526250.17	561.86
T6-2018	8686674.33	526246.57	560.49
T7-2015	8686580.26	525857.56	615.80
T7-2017	8686579.33	525858.40	615.81
T8-2017	8686471.51	525523.83	649.70

Table A.3.: Difference of Northing, Easting and Elevation between the open source and Trimble Business Center values.

Name	Difference Northing [m]	Difference Easting [m]	Difference Elevation [m]
BL2-2016	-0.01	-0.01	-0.03
BL2-2018	-0.01	0.00	0.02
BL3-2016	0.04	-0.04	0.25
BL3-2018	-0.04	0.03	-0.24
BL4-2018	0.00	0.00	0.92
BL4-i-2016	0.01	0.00	-0.10
BL4-ii-2016	0.01	0.01	0.00
BL5-i-2017	0.00	0.03	0.01
BL5-ii-2017	0.00	0.01	0.05
T1-2018	0.06	-0.10	-0.16
T1-i-2017	-0.01	0.02	-0.01
T1-ii-2017	0.14	-0.12	-0.08
T2-2016	-0.45	-0.33	0.24
T2-2018	-0.14	-0.13	-0.73
T2-i-2017	0.00	0.01	-0.05
T2-ii-2017	0.55	0.07	0.51
T3-2017	-0.01	0.01	-0.02
T4-2016	0.00	-0.01	-0.02
T4-2018	-0.32	-0.13	-0.69
T5-2016	0.00	0.01	0.00
T5-2018	0.02	0.00	0.17
T6-2016	0.01	0.00	-0.01
T6-2018	-0.45	-0.31	0.02
T7-2015	0.00	0.00	1.84
T7-2017	-0.04	0.02	-0.14
T8-2017	-0.01	0.01	-0.03

Detailed plots of stake movement

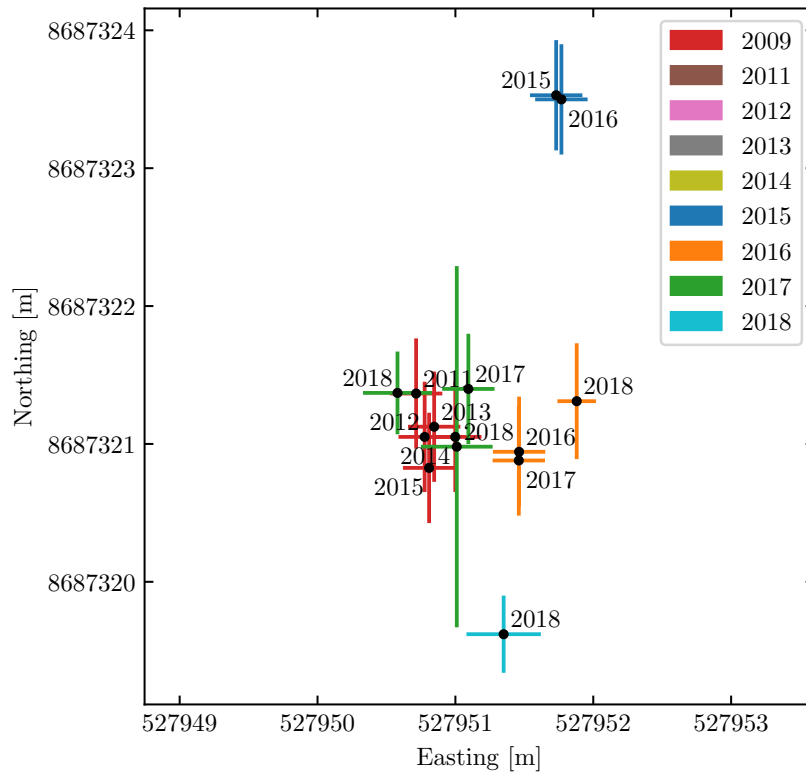


Figure A.1.: Present and past positions of stakes at location T2.

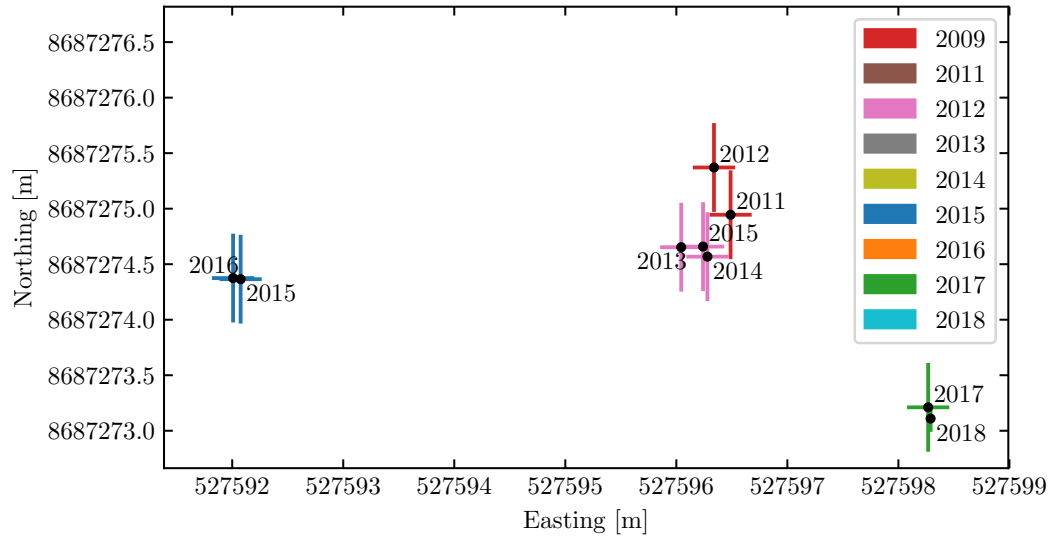


Figure A.2.: Present and past positions of stakes at location T3.

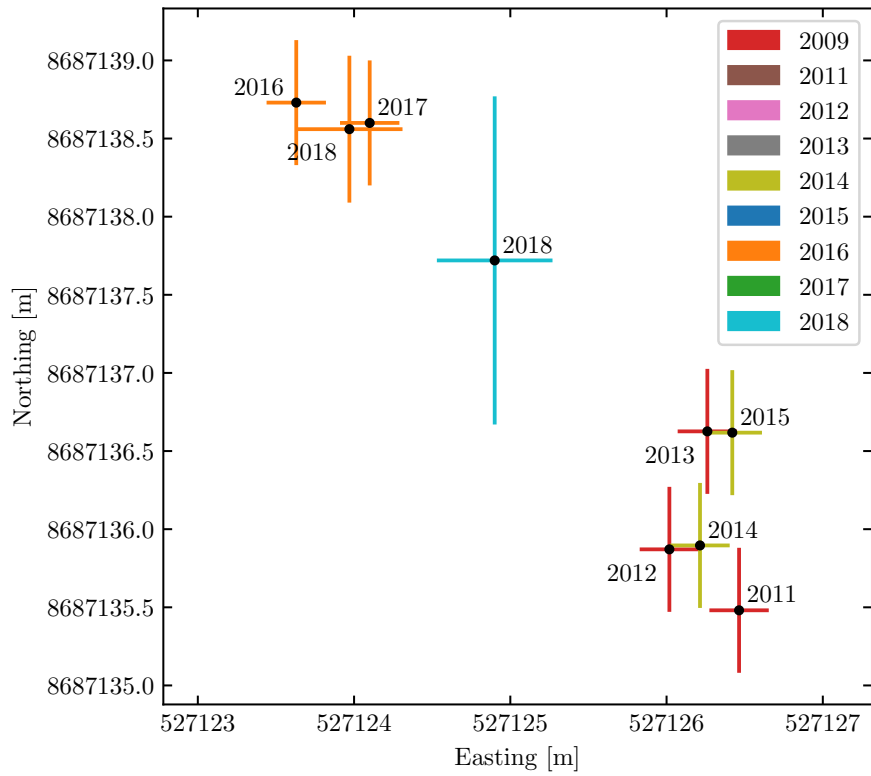


Figure A.3.: Present and past positions of stakes at location T4.

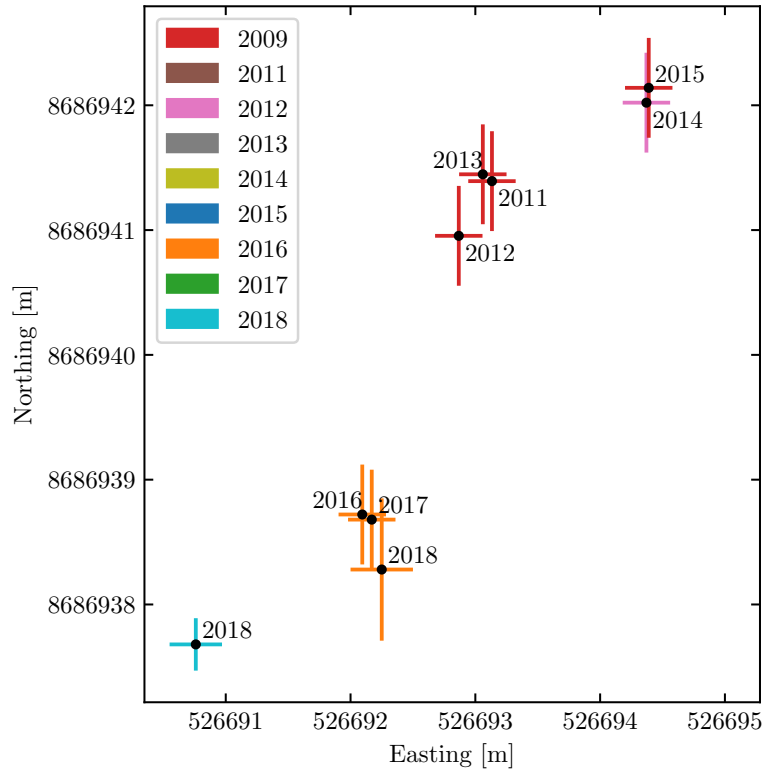


Figure A.4.: Present and past positions of stakes at location T5.

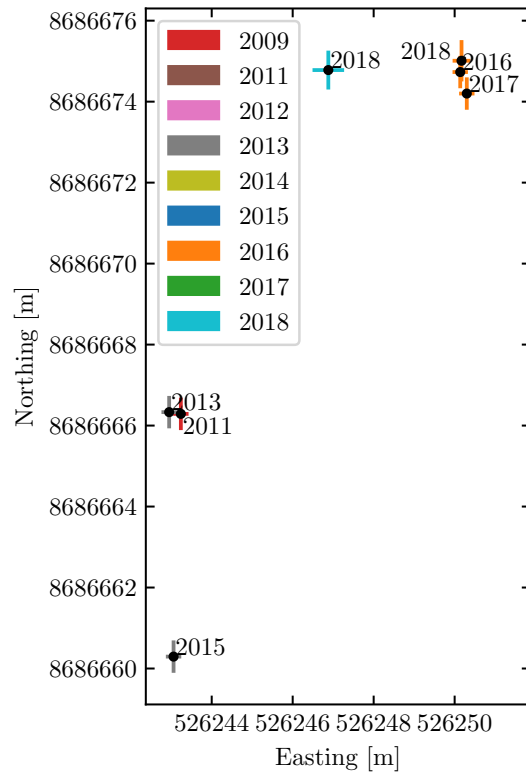


Figure A.5.: Present and past positions of stakes at location T6.

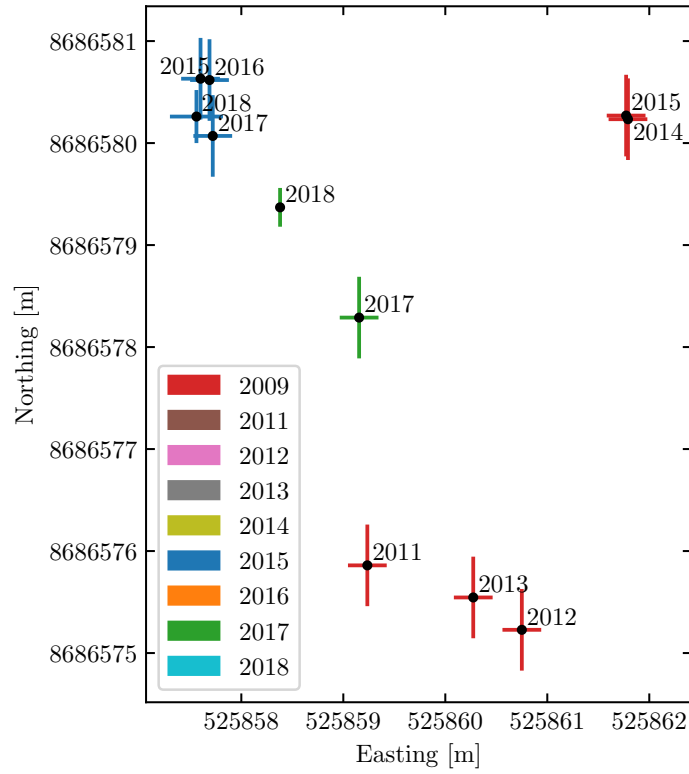


Figure A.6.: Present and past positions of stakes at location T7.

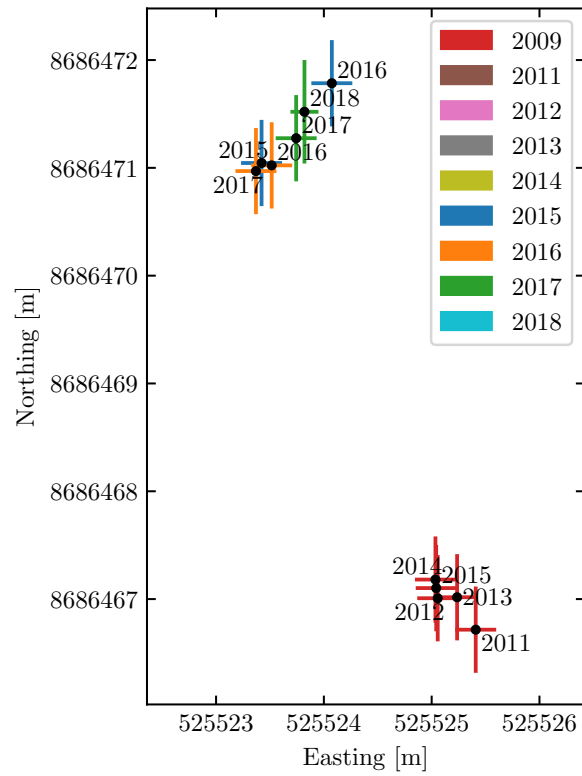


Figure A.7.: Present and past positions of stakes at location T8.

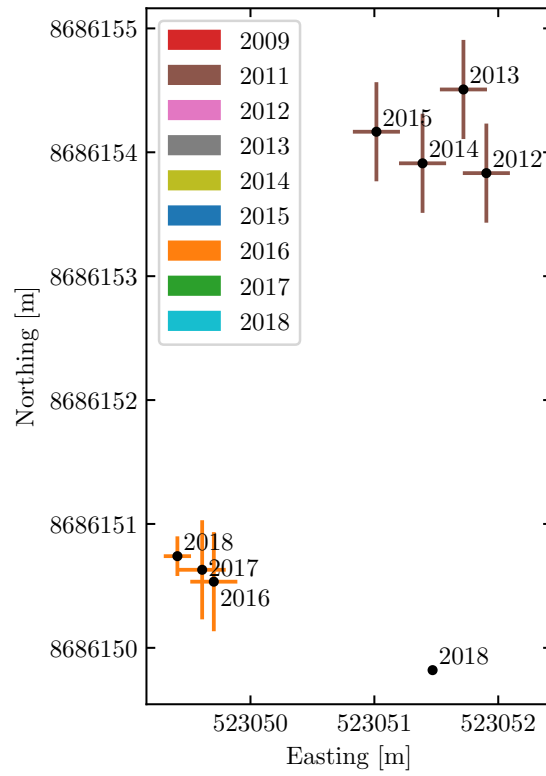


Figure A.8.: Present and past positions of stakes at location BL2.

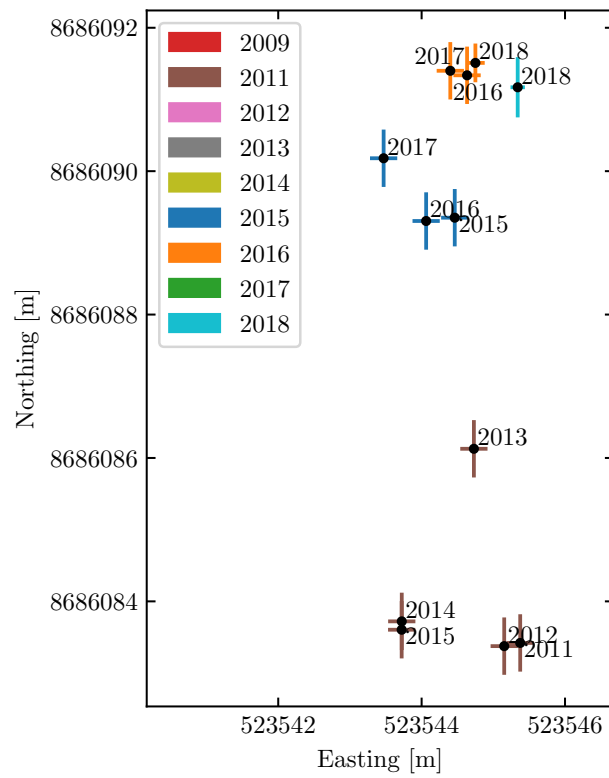


Figure A.9.: Present and past positions of stakes at location BL3.

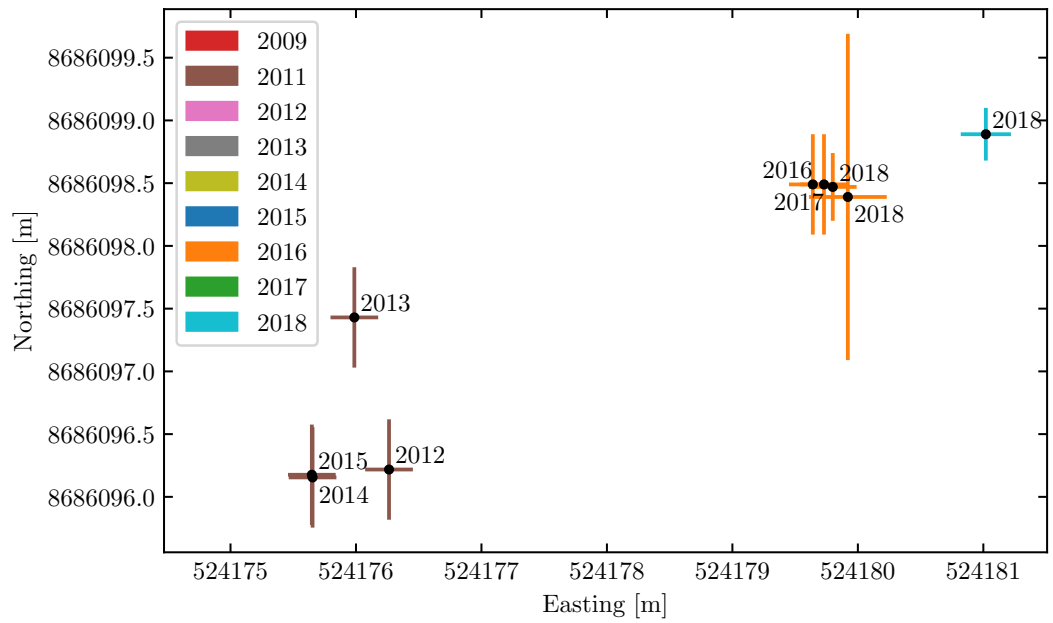


Figure A.10.: Present and past positions of stakes at location BL4.

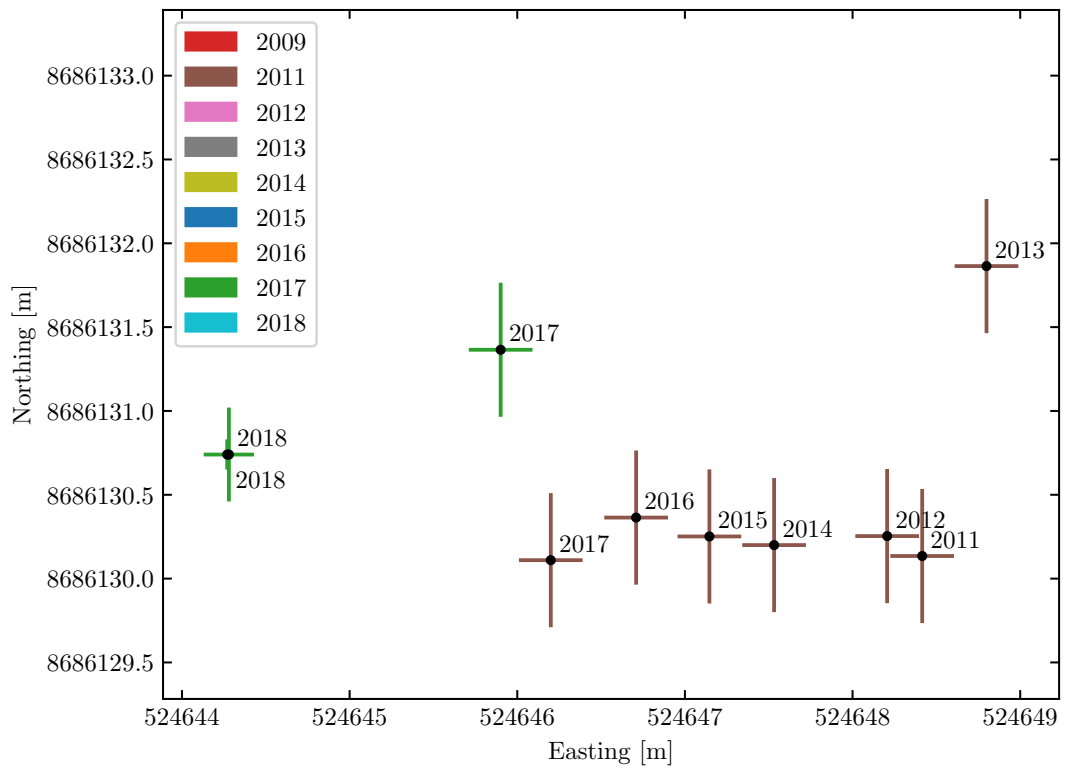


Figure A.11.: Present and past positions of stakes at location BL5.

1 . Ice velocity measured by differential GPS

Appendices, Bibliography; Ice, A Appendix

01	Chris Borstad	Page 4
	30/4/2018 20:35	
	Nye (1952)	
02	Unknown Unknown	Page 4
	30/4/2018 20:35	
03	Chris Borstad	Page 4
	30/4/2018 20:36	
	Glen (1955)	
04	Unknown Unknown	Page 4
	30/4/2018 20:36	
05	Chris Borstad	Page 5
	30/4/2018 20:37	
	(Greve, 2009)	
06	Unknown Unknown	Page 5
	30/4/2018 20:37	
07	Chris Borstad	Page 8
	30/4/2018 20:41	
	you haven't stated yet what these "other" uncertainties are	
08	Unknown Unknown	Page 8
	30/4/2018 20:41	
09	Unknown Unknown	Page 8
	30/4/2018 20:41	

10	Chris Borstad	Page 10
	30/4/2018 20:43 found	
11	Unknown Unknown	Page 10
	30/4/2018 20:43	
12	Chris Borstad	Page 10
	30/4/2018 20:44 shielded	
13	Unknown Unknown	Page 10
	30/4/2018 20:44	
14	Chris Borstad	Page 10
	30/4/2018 20:44 held	
15	Unknown Unknown	Page 10
	30/4/2018 20:44	
16	Unknown Unknown	Page 10
	30/4/2018 20:44	
17	Unknown Unknown	Page 11
	30/4/2018 20:47	
18	Chris Borstad	Page 11
	30/4/2018 20:47 why such a big gap here?	
19	Chris Borstad	Page 11
	30/4/2018 20:47 Figure	
20	Unknown Unknown	Page 11
	30/4/2018 20:47	

21	Unknown Unknown	Page 12
	30/4/2018 20:48	
22	Unknown Unknown	Page 12
	30/4/2018 20:48	
23	Chris Borstad	Page 12
	30/4/2018 20:48 whole	
24	Unknown Unknown	Page 12
	30/4/2018 20:48	
25	Chris Borstad	Page 14
	30/4/2018 20:49 Sec	
26	Unknown Unknown	Page 14
	30/4/2018 20:49	
27	Chris Borstad	Page 14
	30/4/2018 20:50 Table	
28	Unknown Unknown	Page 14
	30/4/2018 20:50	
29	Chris Borstad	Page 15
	30/4/2018 20:51 cosine	
30	Unknown Unknown	Page 15
	30/4/2018 20:50	
31	Chris Borstad	Page 20
	30/4/2018 20:54 relation	

32	Unknown Unknown	Page 20
	30/4/2018 20:54	
33	Chris Borstad	Page 20
	30/4/2018 20:54	
	year's	
34	Unknown Unknown	Page 20
	30/4/2018 20:54	
35	Unknown Unknown	Page 22
	30/4/2018 20:55	
36	Chris Borstad	Page 22
	30/4/2018 20:55	
	subscripts	
37	Unknown Unknown	Page 22
	30/4/2018 20:55	
38	Chris Borstad	Page 23
	30/4/2018 20:56	
	linearly	
39	Unknown Unknown	Page 23
	30/4/2018 20:56	
40	Chris Borstad	Page 25
	30/4/2018 20:57	
	very nice! seems to line up reasonably well with the mass balance record...	
41	Chris Borstad	Page 28
	30/4/2018 20:58	
	chosen	
42	Unknown Unknown	Page 28
	30/4/2018 20:58	

30/4/2018 20:58
different

30/4/2018 20:58